Diptera-specific Daedalus controls Zucchini endonucleolysis in piRNA biogenesis independent of exonucleases

Yuica Koga, Shigeki Hirakata, Mayu Negishi, Hiroya Yamazaki, and Mikiko C. Siomi*

Department of Biological Sciences, Graduate School of Science, The University of Tokyo, Tokyo 113-0032, Japan

*Correspondence: siomim@bs.s.u-tokyo.ac.jp

Summary

piRNAs protect germline genomes and maintain fertility by repressing transposons. Daedalus and Gasz act together as a mitochondrial scaffold for Armitage, a necessary factor for Zucchini-dependent piRNA processing. However, the mechanism underlying this function remains unclear. Here, we find that the roles of Daedalus and Gasz in this process are distinct, although both are necessary: Daedalus physically interacts with Armitage, whereas Gasz supports Daedalus to maintain its function. Daedalus binds to Armitage through two distinct regions, an extended coiled-coil identified in this study, and a SAM. The former tethers Armitage to mitochondria, while the latter controls Zucchini endonucleolysis to define the length of piRNAs in an exonuclease-independent manner. piRNAs produced in the absence of Daedalus SAM do not exhibit full transposon silencing functionality. Daedalus is Diptera specific. Unlike *Drosophila* and mosquitoes, evolutionarily more complex species, such as mice, rely on exonucleases after Zucchini processing to specify the length of piRNAs.

Keywords

Armitage, Daedalus, Gasz, piRNA, Zucchini, AmTEC, extended coiled-coil

Introduction

In *Drosophila* ovarian somatic cells (OSCs), PIWI-interacting RNAs (piRNAs) associate with one of the PIWI members, Piwi, in the cytoplasm to form the piRNA-induced silencing complex (piRISC).[1–4] piRISC then co-transcriptionally represses transposons in the nucleus. The vast majority of piRNAs in OSCs originate from the piRNA cluster, *flamenco* (*flam*).[5] The *flam* locus contains numerous transposon remnants, most of which

have an orientation opposite to the direction of transcription. Therefore, piRNAs can naturally hybridize to target mRNAs through RNA–RNA base pairing.[5,6] After nuclear processing, including splicing,[7] the *flam* transcripts are exported to the cytoplasm where they bind to female sterile (1) Yb (Yb) via *cis*-elements embedded in the RNAs. This interaction induces the assembly of non-membranous organelle Yb bodies through phase separation, which accelerates subsequent steps in the piRNA processing.[8,9]

At this point, the *flam* transcripts are coarsely digested by an unknown factor, generating numerous 5′ ends. Piwi binds one-to-one to these 5′ ends via the MID domain and becomes the Piwi-piRISC precursor (pre-Piwi-piRISC).[10,11] Concomitantly, the RNA helicase Armitage (Armi) binds to the complex, allowing pre-Piwi-piRISC to exit Yb bodies and move to the mitochondrial surface where the endonuclease Zucchini (Zuc) awaits to process the complex.[12] Zuc has a transmembrane (TM) region, which localizes Zuc to the outer membrane of mitochondria.[13–16] After Zuc RNA cleavage releases mature Piwi-piRISC from pre-Piwi-piRISC, nascent Piwi binds to the remaining piRNA precursor through its 5′ end, generating a new pre-Piwi-piRISC in Yb body-independent and Zuc-dependent manners.[17,18] This mechanism of sequential generation of Piwi-piRISC from a single piRNA precursor is known as phasing.[17,18] Piwi-piRISC is then transported to the nucleus,[19] where it associates with nascent transposon transcripts and suppresses transcription in concert with multiple cofactors, such as Gtsf1/Asterix and Maelstrom.[20–27]

An RNAi-based gene screen performed in *Drosophila* ovaries identified many factors acting in the piRNA pathway, including Gasz and Daedalus (Daed).[28] Both proteins have a TM, like Zuc, and they form a heteromeric complex that acts in concert with Armi to support Zuc cleavage in piRNA maturation.[12,29,30] However, the molecular

57 details of this process, especially the function of Daed, remain unclear.

58 In this study, we found that Daed interacts with Armi through two distinct regions,
59 the extended coiled-coil (eCC) identified in this study, and the sterile α motif (SAM). We
60 also show that Daed interacts with Gasz by forming a helical barrel using the two α-
61 helixes present in each of Daed and Gasz. Through this interaction, Daed stabilizes Gasz,
62 but not *vice versa*. Furthermore, we found that the Armi–Daed interaction through Daed
63 eCC tethers Armi to mitochondria, while the Armi–Daed interaction through SAM controls
64 Zuc endonucleolysis to specify the length of piRNAs in an exonuclease-independent
65 manner. piRNAs produced in the absence of Daed SAM became atypically long and their
66 function in transposon silencing was attenuated. Evolutionarily more complex species,
67 such as mice, possess exonuclease, PNLDC1, but not Daed. Mouse piRNAs, which are
68 atypically elongated in the absence of PNLDC1, do not exhibit full functionality in
69 transposon silencing. These findings indicate that piRNA length specification, which is
70 crucial for transposon repression, is conserved between species, but that the means of
71 piRNA length specification differ between species.

72

73 **Results**

74 **Daed and Gasz bind with each other via their respective eCC domains**

75 According to the current model, the Daed–Gasz heterodimer tethers Armi bound to pre-
76 Piwi-piRISC to mitochondria for Zuc-dependent piRNA processing.[12,29,30] In this study,
77 we first predicted the higher-order structure of the Daed–Gasz heterodimer using
78 AlphaFold2[31,32] (Figure 1A). This indicated that both Gasz and Daed have two α-helixes
79 and that the coiled-coil structure composed of these four α-helixes is the center of the
80 Daed–Gasz association (Figure 1B). Daed has SAM, coiled-coil (CC), and TM domains,

81 and Gasz has ankyrin repeats (ARs), SAM, and TM domains.[12,29] The predicted
82 structures of Daed and Gasz showed that the second of the two α-helixes (Ala191–
83 His235) of Daed roughly overlaps with the CC domain (Thr206–Ser234) and that the two
84 α-helixes in Gasz (Phe345–Glu374 and Glu383–Ser412) are present between the SAM
85 and TM domains (Figure 1C). The amino acid sequence-based prediction of the CC
86 region[33] also roughly overlaps with the tandem α-helix regions (Figure S1A), supporting
87 the AlphaFold2 prediction. We propose that the two tandem α-helixes present in both
88 Gasz and Daed are referred to as extended coiled-coil (eCC) domains (Figure 1C).
89 The CC domain of Daed is the region that binds to Gasz.[29] To identify the region
90 of Gasz responsible for binding to Daed we expressed deletion mutants of Gasz in OSCs
91 lacking endogenous Gasz and then performed immunoprecipitation assays. Three of the
92 Gasz deletion mutants, ΔAR1-3, which lacks the first three ARs, ΔAR4-6, which lacks
93 the second three ARs, and ΔSAM, bound to Daed as efficiently as wild-type (WT) Gasz
94 did, but the other mutant, Δα-H2, lacking the second α-helix of eCC did not (Figures 1D
95 and S1B). These results indicate that the respective eCC domains of Daed and Gasz
96 are responsible for the Daed–Gasz association, consistent with the predicted structure.
97
98 **Daed stabilizes Gasz via protein–protein interaction**
99 To verify whether Daed is required for piRNA biogenesis in cultured OSCs, we depleted
100 intracellular Daed by RNA interference (RNAi) and conducted northern blotting. In control
101 OSCs, both *idefix* piRNA (a representative nongenic piRNA) and *traffic jam* (*tj*) piRNA (a
102 representative genic piRNA) were detected as expected (Figure S2A).[12] However, in the
103 absence of Daed, their piRNA precursors (pre-piRNAs) accumulated aberrantly, while
104 mature piRNAs were barely detected (Figure S2A), as in OSCs lacking Gasz.[12] This

105 indicates that both Gasz and Daed are essential for piRNA maturation in OSCs.

106 Western blotting confirmed that RNAi was effective at depleting Daed and Gasz
107 in OSCs (Figure 2A). We also found that, when Daed was depleted, levels of Gasz were
108 also markedly reduced, but that levels of Daed were unchanged in the absence of Gasz
109 (Figures 2A and 2B). Such trends were not observed for their mRNA levels (Figure 2C).
110 These results indicate that Daed is required to stabilize Gasz at the protein level, but that
111 Daed is not dependent on Gasz for its stabilization.

112 To investigate which domain of Daed is involved in Gasz stabilization, two
113 deletion mutants of Daed, ΔSAM and ΔCC (part of the second α-helix of the eCC, see in
114 Figure 1C), were expressed in OSCs depleted of endogenous Daed. Levels of Gasz
115 were restored with expression of WT Daed and ΔSAM mutant Daed, but not with ΔCC
116 mutant Daed (Figure 2D). A previous study showed that Daed binds to Gasz via the CC
117 region[29] and together these findings indicate that the Daed–Gasz interaction via their
118 respective eCC domains is crucial for the stabilization of Gasz (Figure 2E). The Δα-H2
119 mutant of Gasz, which lacks the binding domain to Daed, was rather unstable in OSCs,
120 but this was not because of mRNA instability (Figure S2B), supporting the above notion.
121

122 **Daed alone or Gasz alone is insufficient to tether Armi to mitochondria**

123 Armi has at least two roles in piRNA biogenesis in OSCs; one is to transport nascent
124 Piwi to Yb bodies to promote pre-Piwi-piRISC assembly, and the other is to translocate
125 the complex from Yb bodies to mitochondria to promote Zuc-dependent piRNA
126 processing.[12,34] After this second role, Armi returns to the cytosol to repeat these
127 functions, although immunofluorescence shows that Armi appears to be a constant
128 resident of Yb bodies (Control, Figure 2F).[8,12] In the absence of Zuc, Armi signals merged

129 with mitochondrial signals {[I] Zuc knockdown (KD), Figure 2F}. This demonstrates
130 dynamic movement of Armi in OSCs and indicates that Armi remains on the
131 mitochondrial surface when loss of Zuc impairs piRNA maturation.[12] Results from
132 mitochondrial fractionation followed by western blotting were consistent with this
133 statement (Figures 2G and S2C).

134 We then depleted Daed in Zuc-lacking OSCs, where both Daed and Gasz
135 should be absent (Figure 2A). Under these circumstances, as expected, Armi was not
136 retained on mitochondria and appeared in Yb bodies ([II] Zuc KD + Daed KD, Figure 2F).
137 To restore the levels of both Daed and Gasz simultaneously, Flag-Daed was
138 exogenously expressed in the OSCs and western blotting confirmed the recovery of both
139 Daed and Gasz levels (Figures 2G and S2C). Immunofluorescence showed that Armi
140 re-localized to mitochondria ([III] Flag-Daed, Figure 2F). However, when Gasz was
141 forcibly expressed alone in the absence of Daed, Armi remained in Yb bodies ([IV] Flag-
142 Gasz, Figure 2F). A similar result was obtained in OSCs expressing only Daed ([V] Zuc
143 KD + Gasz KD, Figure 2F). These results indicate that Gasz alone or Daed alone is not
144 sufficient to tether Armi to mitochondria. In other words, both Daed and Gasz are
145 required to retain Armi on the mitochondrial surface for Zuc-dependent piRNA
146 processing. Hereafter, the Daed–Gasz heterodimer is referred to as the Armi
147 mitochondrial tethering complex (AmTEC). The behavior of Armi in OSCs under the
148 conditions described above is summarized in Figure S2D.

149

150 **Daed, but not Gasz, binds to Armi via two distinct sites**

151 We next predicted the higher-order structure of AmTEC bound with Armi (Figure 3A).
152 Notably, no significant interaction between Gasz and Armi was observed, but Daed and

153 Armi were bound at two distinct sites: The first site was through the first α-helix of eCC
154 (Phe144–Val177) (Figure 1C), which interacted with the N-terminal region of Armi
155 (Met1–Leu34) (Figures 3A, 3B, and S3A). The second interaction was between the SAM
156 domain of Daed (Figure 1C) and the C-terminal helicase (i.e., UPF1-like family) domain
157 of Armi (Figures 3A, 3C, and S3A).

158 To verify that the Armi–Daed interaction was via the Armi N-terminus (Figure
159 3B), recombinant WT Armi (WT-Flag) and its mutant lacking 34 N-terminal residues
160 (ΔN34-Flag) were subjected to pull-down assays with Daed (Daed ΔTM) as prey. The
161 Daed TM was removed because its inclusion interfered with protein preparation. Under
162 conditions where a negative control, Luciferase (Luc), showed no binding to Daed ΔTM,
163 Armi WT bound to Daed but Armi ΔN34 did not (Figure 3D). This confirms that Armi and
164 Daed interact through the 34 N-terminal residues of Armi. We have previously shown
165 that the Armi ΔN34 mutant (i.e., a shorter isoform of Armi) is unable to leave Yb bodies.[12]
166 The present analysis raises an alternative hypothesis; the Armi ΔN34 mutant may be
167 able to leave Yb bodies but not be tethered to mitochondria because of the absence of
168 Daed binding. This would explain why the shorter Armi isoform is inactive in piRNA
169 biogenesis in OSCs.

170 To verify the Armi–Daed interaction via the Armi UPF1-like helicase domain
171 (Figure 3C), three residues in the domain, Asp1015, Arg1026, and Arg1037 (D-R-R),
172 which appear to be key to the binding, were mutated to Lys-Glu-Glu (K-E-E) and
173 immunoprecipitation assays were conducted (Figure 3E). Quantification of the results
174 indicated that the Armi KEE mutant bound to Daed with approximately 34% of the binding
175 efficiency of WT Armi (Figure 3F). Meanwhile, the Armi ΔN34 mutant bound to Daed with
176 approximately 20% of the binding efficiency of WT Armi. Immunofluorescence showed

177 that the Armi ΔN34 mutant accumulated in Yb bodies more intensely than the KEE
178 mutant in Arm/Zuc-lacking OSCs (Figure 3G). For binding to Daed, Armi may be more
179 dependent on the N-terminal region than on the UPF1-like helicase domain.

180 A lack of Armi in OSCs severely disrupted piRNA production.[16,35] This was
181 almost fully rescued by the expression of WT Armi (Figure 3H). We next expressed the
182 ΔN34 or KEE mutant of Armi as alternatives to the WT. The ΔN34 mutant failed to rescue
183 the disruption to piRNA production, but the KEE mutant partially restored piRNA
184 biogenesis (Figures 3H and S3B). This supports the notion that the N-terminal region of
185 Armi is more important than the C-terminal helicase domain in piRNA biogenesis in
186 OSCs. The strength of the Armi–Daed interaction (Figure 3E) appears to be positively
187 correlated with the function of Armi.

188

189 **The two Armi–Daed associations differ in their functional contributions to piRNA**
190 **biogenesis**

191 piRNAs produced under conditions involving the Armi KEE mutant were notably
192 increased in length by several bases (Figure 3H). We therefore investigated whether a
193 similar phenomenon occurred under conditions involving the Daed ΔSAM mutant, given
194 that the SAM domain is the binding partner of the UPF1-like helicase domain of Armi.
195 Indeed, in cells expressing the Daed ΔSAM mutant as an alternative to endogenous
196 Daed, Piwi-bound piRNAs became several bases longer and their levels were lower than
197 those in cells expressing WT Daed, but higher compared with cells lacking endogenous
198 Daed (Figures 4A and S4A).

199 To examine how the lack of binding between Daed SAM and Armi UPF1-like
200 helicase domain actually affects piRNA biogenesis, we sequenced and analyzed Piwi-

201 bound piRNAs in OSCs expressing Daed ΔSAM and compared the results with those
202 from OSCs expressing WT Daed (Figures 4A and S4A). This length distribution of
203 piRNAs was indeed shifted towards the longer fractions when they were produced in
204 cells lacking the Daed SAM domain (Figure 4B). This trend was also observed when
205 piRNAs were subdivided by target transposons (Figure S4B). In contrast, piRNA-
206 mapped transposons were essentially unchanged (Figure S4C). This seems reasonable
207 given that piRNAs are produced from *flam* in both cases. Furthermore, the 1U bias[5,36]
208 and piRNA phasing[17,18] were similarly observed in both libraries (Figures 4C and 4D).
209 The β-elimination experiments showed the 3′ ends of the piRNAs to be modified with 2′-
210 *O*-methylation in both cases, unlike Argonaute 1 (Ago1)-bound miRNAs (Figure 4E).[37,38]
211 However, it should be noted that non-negligible amounts of Piwi immunofluorescence
212 remained in the cytoplasm when Daed ΔSAM was expressed in OSCs lacking
213 endogenous Daed (Figure 4F).

214 piRNA loading is essential for Piwi nuclear localization.[19,34] Therefore, we next
215 examined the piRNA binding status of cytoplasmic and nuclear Piwi. In contrast to
216 nuclear Piwi, which was bound to piRNAs even in the long fraction, cytoplasmic Piwi was
217 bound to few piRNAs (Figure S4D). This indicates that piRNAs produced under the
218 ΔSAM conditions can localize Piwi to the nucleus as piRISC, regardless of length, but
219 are insufficient to convert all Piwi to functional Piwi-piRISC. Consistent with this,
220 transposons were not fully repressed under such conditions (Figures 4G and S4E).
221 These results indicate that the Armi–Daed association via the UPF1-like helicase domain
222 of Armi and the SAM domain of Daed is influential in Piwi-piRISC production and function,
223 although less so than the other Armi–Daed association involving the 34 N-terminal
224 residues of Armi and the eCC domain of Daed.

225

226 **The Armi–Daed interaction via Daed SAM optimizes Zuc endonucleolysis for**
227 **piRNA-mediated transposon repression**

228 To explore the nature of ΔSAM piRNA extension, we selected the 50,000 piRNA 5′ end
229 positions common to the WT and ΔSAM and with high abundance in WT libraries (Figure
230 S4F) and analyzed them further. Heatmaps depicted with their 5′ end positions aligned
231 clearly indicate that ΔSAM piRNAs are more diverse in length. Many of them have some
232 extra bases at the 3′ ends (Figure 4H). This is consistent with the length distribution
233 shown in Figure 4A. There are also a few shorter piRNAs (Figure 4H). The relatively
234 small number of shorter piRNAs may be because of protection by Piwi.

235 To further analyze the effects of Daed SAM loss on piRNAs, we extracted the
236 5′-end positions that dominantly produce 26- and 27-nucleotide (nt) piRNAs in the WT
237 library, and then these positions were classified as "Unchanged" (51,833 positions) and
238 "Elongated" (53,258 positions) according to the absence or presence of 3′-end
239 elongation. piRNAs produced from both 5′-end groups maintained comparable phasing
240 and +1U bias (i.e., 1U bias of piRNAs, real and virtual, immediately following piRNAs
241 verified to bind to Piwi[17,18]) (Figure S4G), indicating that piRNA elongation caused by the
242 loss of Daed SAM is caused by Zuc endonucleolysis.

243 We next sorted piRNAs by their length and aligned them according to the 3′
244 ends of piRNAs. This showed that atypically long piRNAs of around 28–33 nt in the WT
245 library tended to have significantly low U bias near their 3′ ends (U depletion), just
246 upstream of the 5′ ends of the immediately downstream piRNAs, as reported previously
247 (yellow boxes in WT, Figure 4I).[18] This was interpreted as showing that when Zuc cannot
248 find U-rich regions in the piRNA precursors it waits to cleave the substrate until the U-

249 poor region has passed, thereby producing atypically long piRNAs. This also explains
250 why there were fewer 28–33-nt piRNAs in the WT library (Figure 4B). In contrast, there
251 was less notable "U depletion" in 28–33-nt ΔSAM piRNAs (yellow boxes in ΔSAM, Figure
252 4I). In addition, there was a substantial number of 28–33-nt piRNAs in the ΔSAM library
253 (Figure 4B). This indicates that when the Armi–Daed interaction is attenuated because
254 of a lack of Armi–Daed association via Daed SAM (and the UPF1-like helicase domain
255 of Armi), Zuc somehow produces these longer piRNAs more preferentially regardless of
256 the U content in the precursor sequences while maintaining the +1U bias.

257 We simulated the effect of Daed ΔSAM on piRNA production. First, we
258 hypothetically fragmented the sequence of the *flam* locus (21,629,891 to 21,792,731 on
259 the X chromosome; T was converted to U) into 163 piRNA precursors, starting at U and
260 into sizes of 1,000 nt or close to that size. In parallel, the data shown in Figure 4B were
261 fitted to normal distributions. Then we simulated Zuc-dependent piRNA production from
262 their 5′ ends by assuming that Zuc cleavage occurs before U, produces 18–40-nt piRNAs,
263 and follows the normal distributions for WT and ΔSAM. Sequence analysis of the
264 obtained piRNAs (25–34 nt) indicated that U depletion was observed in simulations fitting
265 the WT distribution, starting from 29 nt, but less so in simulations fitting the ΔSAM
266 distribution (Figure S4H). This suggests that Zuc has the potential to produce Piwi-
267 piRISC without following the U-depletion rule.

268 To investigate potential causes of Zuc-dependent precursor cleavage changes
269 in ΔSAM, molecular dynamics simulations were performed using the Armi–AmTEC
270 complex model (Figure 3A) and its Daed ΔSAM version. The distance between the center
271 of mass (CoM) of Armi helicase domain (Ser697–Cys1,148 in Figure S3A) and that of
272 the AmTEC was measured (n=5) and the average value was calculated at all time points

273 along each trajectory (Figures S5A and S5B). This analysis shows that there is little
274 difference in the initial Armi–AmTEC CoM distances between Daed WT and ΔSAM, but
275 as the simulation time progresses, the difference tends to increase for the ΔSAM version
276 (Figure S5C). The statistical analysis also shows that the distribution of CoM distances
277 at all time points for all trajectories shifts to larger values for ΔSAM (Figures S5D). These
278 results suggest that Daed ΔSAM tethers Armi more precariously than Daed WT. Based
279 on these results, we hypothesize that "proper" binding of Armi and Daed via the Daed
280 SAM (and the UPF1-like helicase domain of Armi) is critical for maintaining the distance
281 between Armi and the scaffold complex, the loss of which would obscure the location of
282 piRNA precursor cleavage by Zuc, negatively influencing Piwi-piRISC production.

283 We also sequenced and analyzed Piwi-bound piRNAs in OSCs expressing the
284 Armi KEE mutant or WT Armi (Figures 3H and S3B). We found that piRNAs in the Armi
285 KEE library were also several bases longer than the Armi WT piRNAs and retained 1U
286 bias (Figures S6A and S6B). Heatmaps showed that the KEE piRNAs also exhibited
287 characteristics of 3′ end elongation (Figure S6C). These results further support our notion
288 that the SAM domain of Daed and the UPF1-like helicase domain of Armi are the binding
289 partners and that the Armi–Daed interaction is indispensable to optimize Piwi-piRISC
290 maturation by Zuc and piRISC function in OSCs (Figure S6D).
291

292 **Daed is Diptera-specific and controls Zuc cleavage in a Nibbler-independent**
293 **manner**

294 Armi and Gasz are widely conserved among species from invertebrates to vertebrates,
295 but Daed is unique to the Diptera order, which is composed of Brachycera suborder,
296 which includes *Drosophila* and other fly species, and Nematocera suborder which

297 includes mosquitoes (Figures 5A, S7A, and S7B). In contrast, other species not
298 belonging Diptera order do not appear to have Daed orthologs.[39]

299 In mice, primary piRNA biogenesis occurs in the inter-mitochondrial cement,
300 where Armi homolog, MOV10L1, Gasz homolog, ASZ1, Zuc homolog, PLD6, and TDRD
301 proteins play a role in piRNA production: MOV10L1 binds to PIWI proteins (MILI, MIWI
302 and MIWI2) and piRNA precursors and contributes to piRNA biogenesis through its
303 helicase activity.[40,41] ASZ1 is essential for the production of MILI-bound piRNAs in mice[42]
304 and is thought to tether MOV10L1 to mitochondria, together with TDRD proteins, such
305 as TDRD1, to promote MIWI-piRISC production.[40,41]

306 We expressed both MOV10L1 and ASZ1 in OSCs and performed
307 immunoprecipitation. The MOV10L1–ASZ1 interaction was detected to a similar extent
308 in both normal OSCs and OSCs lacking intracellular Daed (Figures 5B and 5C).
309 Immunofluorescence confirmed this; the expression of ASZ1 was sufficient for the
310 mitochondrial localization of MOV10L1, independent of the presence of intracellular
311 Daed (Figure 5D). This indicates that the MOV10L1–ASZ1 interaction and MOV10L1
312 tethering is Daed-independent, while the Armi–Gasz interaction and Armi tethering in
313 *Drosophila* required Daed. These results also indicate that the Armi–Gasz association,
314 at least in OSCs, does not require other factors present in mouse testis. ASZ1 was stable
315 in OSCs lacking endogenous Daed (Figure 5C), unlike Gasz (Figure 2A), indicating that
316 the molecular system that actively degrades Gasz in the absence of Daed does not act
317 on ASZ1.

318 Why did *Drosophila* acquire Daed during evolution? In mice, poly(A)-specific
319 ribonuclease-like domain containing 1 (PNLDC1), a homolog of poly(A)-specific
320 ribonuclease (PARN), trims the 3′ ends of piRNAs and piRNAs are elongated after

321 PNLDC1 loss of function.[43,44] Mutation in PNLDC1 reduces LINE-1-targeting piRNAs and
322 mislocalizes MIWI2 to the cytoplasm, leading to LINE-1 derepression. This was nearly
323 equal to what we observed in this study with the *Drosophila* Daed ΔSAM mutant.
324 However, PNLDC1 is not conserved in the majority of Diptera order species.[45] Papi is
325 the *Drosophila* ortholog of TDRKH, which, in mice, acts as a scaffold for PNLDC1 and
326 whose functional inhibition causes piRNA elongation.[46,47] However, consistent with
327 previous studies using Papi mutant flies,[45] its depletion had little effect on piRNA length
328 in OSCs (Figure 5E).

329 The 3′-to-5′ exonuclease, Nibbler (Nbr), trims both miRNAs and piRNAs in
330 *Drosophila* and mosquitoes,[45,48–50] but the pre-piRNAs that undergo trimming are minor
331 in mosquitoes, and the loss of Nbr barely affected the length of Piwi-bound piRNAs in
332 the *Drosophila* ovary.[45] Our study confirmed this; namely, Nbr depletion in OSCs had
333 little effect on the piRNA length (Figure 5F). This indicates that Nbr may function in the
334 trimming of miRNAs, but not piRNAs, in OSCs. The lack of a marked increase in +1U
335 signal in piRNAs elongated in the Daed ΔSAM mutant (Figures 4D and S4G) also
336 supports this view.

337 In contrast, Armi D-R-R, which was essential for the regulation of Zuc cleavage
338 in *Drosophila*, is highly conserved in the fly species that lack PNLDC1/PARN and have
339 Daed (Figure S8). These results indicate that *Drosophila,* and its closely related species,
340 may have acquired Daed after losing PNLDC1/PARN during evolution, and that they
341 may also have acquired the ability to produce mature piRNAs without further trimming
342 by exonucleases by allowing Armi to bind directly to Daed (Figure 5G).

343

344 **Discussion**

345 This study revealed that Daed and Gasz bind to each other via their eCC domains, both
346 of which are composed of two α-helixes that assemble into a stable helical barrel
347 consisting of all four of these α-helixes. When Daed lacks the second α-helix in the eCC
348 domain, the Daed–Gasz interaction is disrupted and Gasz becomes destabilized,
349 illustrating the importance of Daed in Gasz stabilization (Figure 2E). This also shows that
350 the intracellular level of Gasz is strictly regulated by the intracellular level of Daed,
351 indicating that OSCs do not tolerate the presence of Gasz alone. In contrast, OSCs do
352 tolerate the presence of Daed alone. However, Daed, in the absence of Gasz, failed to
353 anchor pre-Piwi-piRISC to mitochondria via Armi. Gasz is therefore complicit in the role
354 of Daed, although the contribution of Gasz to the direct binding of Daed to Armi appears
355 to be minimal.

356 Lack of binding through the Daed SAM did not completely abolish the Armi–
357 Daed association but resulted in aberrant Zuc function (Figure S6D). Under such
358 conditions, Piwi-bound piRNAs were atypically long because of extra bases at the 3′
359 ends, and there was no notable U depletion, a typical feature of piRNAs in normal OSCs.
360 In normal OSCs, atypically long piRNAs are produced only when piRNAs of typical sizes
361 cannot maintain the +1U bias. In contrast, in OSCs expressing Daed ΔSAM, Zuc shows
362 "relaxed selectivity" in terms of nucleotides and length and tends to produce longer
363 piRNAs, even under conditions where it can produce shorter (i.e., normal size) piRNAs
364 with the +1U bias, albeit in relatively small quantities. This could be because of the timing
365 of Zuc RNA cleavage was shifted slightly downstream of the precursor while the
366 preference for cleavage before U was conserved. Recombinant Zuc did not show U
367 selectivity,[15] indicating that, *in vivo*, Zuc may rely on a cofactor to confer U selectivity,
368 and that this cofactor may not require the Armi–Daed association to execute its function.

369 Interestingly, Piwi could accept those longer piRNAs produced under the ΔSAM
370 conditions and localized to the nucleus as Piwi-piRISC. At the same time, however,
371 nonnegligible amounts of Piwi remained in the cytoplasm because of the lack of piRNA
372 loading, which resulted in transposon derepression. This means that the ability of Daed
373 to interact with Armi via the SAM domain, in addition to the binding via the first α-helix in
374 the eCC domain, is essential not only to define the positions of Zuc cleavage, but also
375 to produce enough Piwi-piRISC for transposon repression in OSCs. It is worth noting
376 that no such regulatory factor has been identified to date.

377 Armi is unique in that it plays multiple roles in piRNA biogenesis. First, Armi
378 delivers unloaded Piwi to Yb bodies, facilitating the assembly of pre-Piwi-piRISC in these
379 organelles. In Yb bodies, Armi binds to pre-Piwi-piRISC and translocates the complex to
380 mitochondria. There, Armi anchors pre-Piwi-piRISC to the mitochondria by binding to
381 Daed. This allows Zuc to process pre-Piwi-piRISC into mature Piwi-piRISC. Armi is
382 therefore a factor that always accompanies Piwi and encourages it along the pathway to
383 develop into Piwi-piRISC.

384 Armi is an RNA helicase protein, and its RNA helicase activity is required to
385 avoid stochastic interactions with abundant mRNAs.[51] In contrast, up to this point, the
386 RNA helicase activity of Armi does not seem to be required for the piRNA precursors,
387 rather its activity would be inhibitory. However, in the absence of this activity, especially
388 for phasing, the sequential generation of Piwi-piRISC from a single piRNA precursor
389 would not occur. It is possible that an inhibitor of the RNA helicase activity of Armi is
390 present in OSCs and functions until phasing, but, upon binding to Armi, Daed would lose
391 its function allowing phasing to occur.

392 Animals that reproduce sexually retain the highly conserved piRNA mechanism

393 and use it to maintain their fertility by repressing transposons. However, the evolutionary
394 rate of many piRNA factors, including Armi, is rapid,[52,53] suggesting that these species
395 have adapted the machinery to their specific endogenous and exogenous environments.
396 Coevolution of piRNAs and transposons through host–pathogen arms races has been
397 proposed as a background to this process.[54] Although flies and mosquitoes belong to
398 the same Diptera order, the piRNA pathway factors are highly diverse.[55] On the other
399 hand, our observation that Daed is conserved among Diptera species may suggest the
400 importance of this factor in Dipteran piRNA biogenesis pathway where PNLDC1 is lost.
401

402 **Author contributions**

403 YK and MN performed biochemical experiments. YK, SH, and HY performed
404 bioinformatic analyses, computational structural prediction, simulation, and calculation.
405 MCS supervised and discussed the work and wrote the manuscript with the other authors.
406

407 **Acknowledgments**

408 We thank Y. Namba, Y.W. Iwasaki, H. Nishimasu, and S. Kuraku for useful discussions,
409 K. Kudo, T. Yasuda, and Y. Fukushima for technical assistance with the molecular
410 dynamics simulation, and T. Fujisawa, T. Kinoshita, and H. Ishizu for technical
411 assistance with the biochemical analysis. This study was supported by MEXT KAKENHI
412 Grant Numbers JP19H05466 (to MCS), JP22K15056 (to SH), JP23K14141 (to HY), and
413 JP22KJ1122 (to YK). Some computations were performed on the NIG supercomputer at
414 ROIS National Institute of Genetics.
415

416 **Conflict of interest**

417 The authors declare no competing interests.

418

419 **Figure legends**

420 **Figure 1. Daed and Gasz interact via their respective eCC domains**

421 (**A**) Predicted structure of the Daed–Gasz heterodimer by AlphaFold2. (**B**) Magnification
422 of the region indicated by the dotted line box in (**A**). The structure is shown from two
423 directions. (**C**) Domain structures of Daed and Gasz. Peptide sequences of eCCs of
424 Daed and Gasz are also shown. (**D**) Immunoprecipitation (Flag IP) and western blotting
425 show that one of the Gasz mutants, Δα-H2, fails to bind to Daed in OSCs lacking
426 endogenous Gasz. Flag-Luc: negative control. *: Heavy chains. The domain structures
427 Gasz WT and deletion mutants are also shown.

428

429 **Figure 2. Daed stabilizes Gasz via interaction and both Daed and Gasz are**
430 **essential for the mitochondrial tethering of Armi**

431 (**A**) Western blotting shows the high efficiency of knockdown (KD) of Daed and Gasz in
432 OSCs. Daed KD also destabilizes Gasz, but not *vice versa*. β-Tub: loading control. (**B**,
433 **C**) The statistics of western blotting signals (n=3; **A**) and the mRNA expression levels of
434 *Daed* and *Gasz* upon Daed KD and Gasz KD (n=3). Signal intensities (**B**) or values (**C**)
435 relative to control (EGFP KD) were normalized with those of β-Tub or *rp49*, respectively,
436 and presented as mean values±SE. **: p <0.01; ***: p <0.005; n.s.: p >0.05 [*t*-test
437 (unpaired, two-sided)]. (**D**) Western blotting showing the levels of endogenous Gasz and
438 Flag-Daed (WT and deletion mutants) in OSCs under each condition. β-Tub: loading
439 control. The domain structures of Daed WT and mutants are shown. (**E**) Model of Gasz
440 stabilization by Daed. (**F**) Subcellular localization of Armi (green) in OSCs under various

441 conditions, [I] to [V]. Mitochondria (mito) and Yb bodies (Yb; white arrowheads) are
442 shown in magenta. The signals of Flag-Gasz and Flag-Daed are shown in yellow. Images
443 in the same vertical row are identical cells. Control: normal OSCs. DAPI (blue): nuclei.
444 Scale bar 5 μm. (**G**) Western blotting shows the levels of endogenous Armi, Gasz, Daed,
445 Flag-Gasz (orange asterisk), and Flag-Daed (blue asterisk) in total lysates (total) and
446 mitochondrial fractions (mito) under conditions [I] to [VI]. For the efficiency of cell
447 fractionation, see Figure S2C.
448
449 **Figure 3. Daed interacts with Armi through two sites, each contributing differently**
450 **to piRNA biogenesis**
451 (**A**) The structure of the Armi–AmTEC complex predicted by AlphaFold2. Gray lines:
452 virtual lipid bilayers. The domain structures of Armi, Daed, and Gasz are also shown. (**B**)
453 Magnification of the "B" region in (**A**). The 34 N-terminal residues of Armi (N34) interacts
454 with the first α-helix of Daed eCC. (**C**) Magnification of the "C" region in (**A**). The Armi
455 UPF1-like helicase domain interacts with Daed SAM. Asp1015, Arg1026, and Arg1037
456 of Armi are shown in blue. (**D**) *In vitro* pull-down assays show Armi WT-Flag, but not
457 Armi ΔN34-Flag, binding to Daed (Daed ΔTM-His). Luc-Flag: negative control. *: Heavy
458 and light chains. (**E**) Immunoprecipitation (Flag IP) and western blotting show the
459 amounts of endogenous Daed co-immunoprecipitated with Armi WT-Flag, ΔN34-Flag,
460 and KEE-Flag. Luc-Flag: negative control. The domain structures of Armi WT and its
461 mutants are shown below. Asp1015, Arg1026, and Arg1037 mutated in the KEE mutant
462 are also shown. The peptide sequence of Armi is shown in Figure S3A. (**F**) The statistics
463 of western blotting signals (n=3; **E**). The signals of Daed were normalized with those of
464 Armi and presented as mean values±SE. *: p <0.05; ***: p <0.005 [*t*-test (unpaired,

465 two-sided)]. (**G**) Subcellular localization of Armi WT, ΔN34, and KEE (green) in OSCs
466 lacking endogenous Zuc (Zuc KD) and Armi (Armi KD). Mitochondria (mito; for WT and
467 KEE) and Yb bodies (Yb, white arrowhead; for ΔN34) are shown in magenta. Images in
468 the same vertical row are identical cells. DAPI (blue): nuclei. Scale bar: 5 μm. (**H**) Piwi-
469 bound piRNAs obtained under each condition. Signal intensities (n=3) are normalized as
470 a percentage of the total. The mean (line) and 95% confidence interval (shadow) are
471 shown. The amount of Piwi in each sample is shown at the bottom.
472
473 **Figure 4. The loss of Armi–Daed interaction via Daed SAM obscures Zuc cleavage**
474 **and impairs Piwi-piRISC function**
475 (**A**) Piwi-bound piRNAs obtained under each condition. Signal intensities (n=3) are
476 normalized as a percentage of the total. The mean (line) and 95% confidence interval
477 (shadow) are shown. The amount of Piwi in each sample is shown at the bottom. (**B**)
478 Length distribution of piRNAs (18–40 nt) in Daed WT (green) and ΔSAM (red) libraries
479 (n=3), presented as mean values ± SE. (**C**) Sequence logos representing 11 nt from the
480 5′ end of piRNAs in Daed WT and ΔSAM libraries. (**D**) Heatmaps showing 3′ end counts
481 of piRNAs mapped around the 10,000 most abundant piRNA 5′ ends (lower) and its
482 binary histograms (upper) in Daed WT (left) and ΔSAM (right). (**E**) β-elimination assays.
483 Piwi-bound piRNAs in Daed KD OSCs expressing Daed WT and ΔSAM are shown.
484 Ago1-bound miRNAs are used as positive controls. (**F**) Subcellular localization of
485 endogenous Piwi (green) in Daed KD OSCs expressing Daed WT and ΔSAM (magenta).
486 DAPI (blue): nuclei. Scale bar: 5 μm. (**G**) The expression levels of transposons (*mdg1*,
487 *tabor*, *412*, and *stalker2*) in control OSCs (dark gray), Daed-lacking OSCs (Daed KD;
488 light gray), Flag-Daed WT rescued (WT; green) or Flag-Daed ΔSAM rescued cells

489 (ΔSAM; red) (n=5). Values relative to the control (EGFP KD) were normalized to *rp49*
490 and presented as mean values ± SE **: $p < 0.01$; n.s.: $p > 0.05$ [Wilcoxon rank sum exact
491 test (two-sided)]. (**H**) Heatmaps showing the frequency of the 3′ end positions (red)
492 corresponding to each 5′ end of piRNAs in Daed WT (upper) and ΔSAM (lower) libraries.
493 The 50,000 piRNA 5′ end positions common to both libraries and most abundant in the
494 WT library were used for analysis. (**I**) Sequence logos. piRNAs were sorted by their
495 lengths and aligned according to the 3′ end of the piRNAs (black arrowhead) and its
496 immediately downstream nucleotide is highlighted in green. The U depletion found in 28–
497 33-nt piRNAs in the WT library and the equivalent regions in ΔSAM are highlighted in
498 yellow.
499
500 **Figure 5. Daed is Diptera-specific and controls Zuc cleavage in a Nbr-independent**
501 **manner**
502 (**A**) Protein conservation state of Armi, Gasz, Daed, PNLDC1, Papi, and Nbr in *D.*
503 *melanogaster* and other species. (**B**, **C**) Immunoprecipitation (Flag IP) and western
504 blotting show Myc-ASZ1 binds to MOV10L1 in normal (**B**) and Daed-depleted OSCs (**C**).
505 Luc-Flag: negative control. (**D**) Subcellular localization of Myc-ASZ1 alone or MOV10L1-
506 Flag (green) with Myc-ASZ1 (yellow) in normal (left two row) and Daed-depleted OSCs
507 (right two row). Mitochondria (mito) are shown in magenta. Images in the same vertical
508 row are identical cells. DAPI (blue): nuclei. Scale bar: 5 μm. (**E**, **F**) The efficiency of Papi
509 KD (upper) and Nbr KD (lower) (n=3). Piwi-bound piRNAs in control and Papi-KD (upper)
510 and Nbr-KD OSCs (lower). The amount of Piwi in each sample is also shown. (**G**) Model
511 proposed in this study. Diptera species acquired Daed instead of PNLDC1/PARN during
512 evolution; Daed and Gasz form AmTEC, which stably tethers Armi to the mitochondrial

513 surface via two sites. This allows Zuc to define the length of piRNAs without relying on
514 exonucleases such as PNLDC1/PARN or Nbr. In contrast, in mice, MOV10L1/Armi is
515 tethered solely by ASZ1/Gasz. In this case, Zuc cleavage does not specify piRNA length;
516 therefore, trimming by exonucleases such as PNLDC1/PARN is required after Zuc
517 processing. Blue arrowhead: Zuc cleavage.
518

519 **STAR★Methods**

520 Key resources table

REAGENT or RESOURCE	SOURCE	IDENTIFIER
Antibodies		
Mouse monoclonal antibody Anti-Daed	This study	P3F10
Mouse monoclonal antibody anti-Gasz	Yamashiro et al.[12]	1H7
Mouse monoclonal antibody anti-Armi	Saito et al.[16]	2F8A9
Mouse monoclonal antibody anti-Piwi	Saito et al.[36]	3G11
Mouse monoclonal antibody anti-Piwi	Saito et al.[36]	4D2
Mouse monoclonal antibody anti-Yb	Murota et al.[56]	1G2H3
Mouse monoclonal antibody anti-Ago1	Okamura et al.[57]	1B8
Mouse monoclonal antibody anti-β-Tub	Developmental Studies Hybridoma Bank	Cat#E7; RRID: AB_528499
HSP60 antibody, Clone LK1	StressMarq Biosciences	Cat# SMC-110 (also SMC-110B), RRID:AB_2121277
Anti-Histon H3 antibody – Nuclear Loading Control and ChIP grade	abcam	Cat# ab1791, RRID:AB_302613
Monoclonal anti-Flag M2 antibody	Sigma-Aldrich	Cat# F3165, RRID:AB_259529
Anti-Flag antibody produces in rabbit	Sigma-Aldrich	Cat# F7425, RRID:AB_439687
Anti-c-Myc antibody produces in rabbit	Sigma-Aldrich	Cat# C3956, RRID:AB_439680
anti-mouse IgG (H+L) HRP	Cappel	55558
anti-rabbit IgG HRP-linked	Cell Signaling Technology	Cat#7074, RRID: AB_2099233
Alexa Fluor 488 goat anti-mouse IgG1 antibody	Thermo Fisher Scientific	Cat#A-21121; RRID: AB_2535764

Alexa Fluor 488 goat anti-mouse IgG2b antibody	Thermo Fisher Scientific	Cat# A-21141 (also A21141), RRID:AB_141626
Alexa Fluor 555 goat anti-mouse IgG1 antibody	Thermo Fisher Scientific	Cat# A-21127, RRID: AB_2535769
Alexa Fluor 555 goat anti-mouse IgG2b antibody	Thermo Fisher Scientific	Cat# A21147, RRID:AB_1500897
Alexa Fluor 488 goat anti-rabbit IgG (H+L) antibody	Thermo Fisher Scientific	Cat# A-11008, RRID:AB_143165
Alexa Fluor 633 goat anti-rabbit IgG (H+L) antibody	Thermo Fisher Scientific	Cat# A-21070 (also A21070), RRID:AB_2535731
Bacterial and virus strains		
Escherichia coli Rosetta 2 (DE3)	Novagen	Cat#71397
Chemicals, peptides, and recombinant proteins		
Shields and Sang M3 Insect Medium w/ L-Glutamine	USBiological	Cat#S1013
Fetal Bovine Serum	NICHIREI	Cat#173012
NEBuilder HiFi DNA Assembly Master Mix	New England Biolabs	Cat#E2621X
Ligation high ver.2	Toyobo	Cat#LGK-201
Glutathione Sepharose 4B	Cytiva	Cat#17-0756-01
Phosphate-buffered saline	FUJIFILM Wako Pure Chemical	Cat#048-29805
ClearTrans SP PVDF membranes	Fujifilm Wako Pure Chemical	Cat#033-22453
Clarity Western ECL Substrate	Bio-Rad	Cat#170506
Dynabeads Protein G	Thermo Fisher Scientific	Cat#10009D
RNasin Plus Ribonuclease Inhibitor	Promega	Cat#N2615
T4 Polynucleotide Kinase	New England Biolabs	Cat#M0201L
ISOGEN II	FUJIFILM Wako Pure Chemical	Cat#311-07361
Hybond-N membrane	Cytiva	Cat#RPN303N
VECTASHIELD Antifade Mounting Medium with DAPI	VECTOR LABORATORIES	Cat#H-1200
MitoTracker Orange CMXRos	Thermo Fisher Scientific	Cat#M-7510
SYBR Gold Nucleic Acid Gel Stain	Thermo Fisher Scientific	Cat#S11494
TURBO DNase	Life Technologies	Cat#AM2239

ReverTra Ace qPCR RT master mix	Toyobo	Cat#TYFSQ201
cOmplete ULTRA Tablets, EDTA-free, Protease Inhibitor Cocktail	Roche	Cat#6538282001
RNase A	Roche	Cat#10109142001
Critical commercial assays		
Nucleofector 96-well Shuttle device	Lonza	Cat#AAF-1003S
Nucleofector 2b device	Lonza	Cat#AAB-1001
ChemiDoc XRS Plus System	Bio-Rad	Cat#1708265J1PC
LSM980 laser scanning confocal microscope	Carl Zeiss	Cat#LSM980
StepOnePlus Real-Time PCR system	Thermo Fisher Scientific	Cat#4376598
MiSeq	Illumina	Cat#SY-410-1003
SF Cell Line 96-well Nucleofector Kit	Lonza	Cat#V4SC-3096
QIAseq FastSelect-rRNA Fly Kit	QIAGEN	Cat#333262
PowerUp SYBR Green Master Mix	Thermo Fisher Scientific	Cat# A25743
MiSeq Reagent Kit v3	Illumina	Cat#MS-102-3001
Deposited data		
Raw sequencing data	This paper	GEO: GSExxxxxx
Experimental models: Cell lines		
OSC	Saito et al.[34]	N/A
Oligonucleotides		
Primer sequences	Table S1	N/A
siRNA sequences	Table S2	N/A
Probe sequences	Table S3	N/A
qPCR primer sequences	Table S4	N/A
Recombinant DNA		
pGEX	Cytiva	Cat#28-9546-48
pAc-Flag-Daed WT and mutants	This study	N/A
pAc-Flag-Armi WT	Ishizu et al.[51]	N/A
pAc-Flag-Gasz WT	Yamashiro et al.[12]	N/A
pAc-Flag-Gasz mutants	This study	N/A
pAc-Armi WT-Flag	Yamashiro et al.[12]	N/A
pAc-Armi ΔN34-Flag	Yamashiro et al.[12]	N/A
pAc-Armi KEE-Flag	This study	N/A
pAc-Myc-Luc	gift from H. Ishizu	N/A
pAc- Luc-Flag	Yamashiro et al.[12]	N/A

pAc-Flag-Luc	This study	N/A
pAc-MOV10L1-Flag	This study	N/A
pAc-Myc-ASZ1	This study	N/A
Software and algorithms		
Python (Ver. 3.8.8)	Van Rossum & Drake[58]	RRID:SCR_008394;https://www.python.org
Numpy (Ver. 1.20.1)	Harris et al.[59]	RRID:SCR_008633; https://numpy.org/ja/
Scipy (Ver. 1.6.2)	Virtanen et al.[60]	RRID:SCR_008058; https://scipy.org
Pandas (Ver. 1.2.4)	McKinney[61]	RRID:SCR_018214;https://pandas.pydata.org
R (Ver. 4.3.1)	R Development Core Team[62]	RRID:SCR_001905;https://www.r-project.org
Cutadapt (Ver. 4.0)	Martin[63]	RRID:SCR_011841;https://cutadapt.readthedocs.io/en/stable/
STAR (Ver.2.7.8a)	Dobin et al.[64]	RRID:SCR_004463;https://github.com/alexdobin/STAR
HTSeq (Ver. 0.9.1)	Anders et al.[65]	RRID:SCR_005514;https://htseq.readthedocs.io/en/latest/
bedtools (Ver. 2.30.0)	Quinlan & Hall[66]	RRID:SCR_006646;https://bedtools.readthedocs.io/en/latest/
SAMtools (Ver. 1.9)	Li et al.[67]	RRID:SCR_002105;http://www.htslib.org
deepTools (Ver. 3.3.2)	Ramírez et al.[68]	RRID:SCR_016366;https://deeptools.readthedocs.io/en/develop/
wigToBigWig (Ver. 357)	UCSC	https://www.encodeproject.org/software/wigtobigwig/
ggseqlogo	Wagih.[69]	https://omarwagih.github.io/ggseqlogo/
RSeQC (Ver. 2.6.4)	Wang et al.[70]	RRID:SCR_005275;https://rseqc.sourceforge.net
Fiji (Ver. 2.0.0-rc-69/1.52p)	Schneider et al.[71]	RRID:SCR_002285; https://fiji.sc
seaborn (Ver. 0.12.2)	Waskom et al.[72]	https://seaborn.pydata.org
AlphaFold (Ver. 2.3)	Jumper et al.[32]	https://github.com/google-deepmind/alphafold

UCSF ChimeraX (Ver. 1.6.1)	Pettersen et al.[73]	RRID:SCR_015872;https://www.cgl.ucsf.edu/chimerax/
ISOLDE (Ver. 1.6)	Croll[74]	https://tristanic.github.io/isolde/
CHARMM-GUI Martini bilayer maker (Ver. 3.8)	Jo et al.[75]; Lee et al.[76]; Qi et al.[77]	RRID:SCR_025037;https://www.charmm-gui.org
PPM 3.0 Web Server	Lomize et al.[78]	https://opm.phar.umich.edu/ppm_server
PyMOL (Ver. 2.5.0)	Schrödinger & DeLano	RRID:SCR_000305;http://www.pymol.org/
GROMACS (Version 2021.2)	Abraham et al.[79]	RRID:SCR_014565;http://www.gromacs.org
MDAnalysis (Ver. 2.7.0)	Michaud-Agrawal et al.[79]; Gowers et al. [80]	https://mdanalysis.readthedocs.io/en/latest/index.html
CLUSTAL Omega	Madeira et al.[82]	RRID:SCR_001591;https://www.ebi.ac.uk/jdispatcher/msa/clustalo
iTOL (Ver. 6.9)	Letunic & Bork[83]	RRID:SCR_018174;https://itol.embl.de
ESPript (Ver. 3.0)	Robert & Gouet[84]	https://espript.ibcp.fr
MEGA11	Tamura et al.[85]	RRID:SCR_023017;https://www.megasoftware.net/

Resource availability

Lead contact

Further information and requests for resources and reagents should be directed to and will be fulfilled by the lead contact, Mikiko C. Siomi (siomim@bs.s.u-tokyo.ac.jp).

Materials availability

Plasmids and antibodies generated in this study will be shared by the lead contact upon request.

Data and code availability

The data supporting the findings of this study are available from the corresponding authors upon reasonable request. The datasets produced in this study are available in

532 the following databases: RNA-Seq data: Gene Expression Omnibus GSExxxxxx
533 (https://www.ncbi.nlm.nih.gov/geo/query/acc.cgi?acc=GSExxxxxx).

534 **Experimental model and study participant details**

535 OSCs were cultured at 26°C in Shields and Sang M3 medium (USBiological)
536 supplemented with 10% fetal bovine serum (FBS, NICHIREI), 0.6 mg/mL glutathione, 10
537 mU/mL insulin, and 10% fly extract.[8]

538

539 **Method details**

540 **Plasmid construction**

541 The Daed coding region was amplified from total OSC RNAs by RT-PCR and inserted
542 into pAc-Flag-Armi WT[51] by substituting the Armi coding region using NEBuilder HiFi
543 DNA Assembly Master Mix (New England Biolabs). RNAi-resistant Daed WT and its
544 ΔSAM and ΔCC mutants were generated by inverse PCR, according to the domain
545 structures described in a previous study.[29] To construct the expression vector for GST-
546 Daed ΔTM-His, corresponding coding regions of Daed were cloned into pGEX, after
547 which a His-Tag was added to the C-terminal by inverse PCR. RNAi-resistant Flag-Gasz
548 mutants (ΔAR1-3, ΔAR4-6, ΔSAM, and Δα-H2) were generated by inverse PCR using
549 RNAi-resistant Flag-Gasz WT vector[12] as a template. Vectors for RNAi-resistant Armi
550 WT-Flag and its ΔN34 mutant were previously constructed.[12] The Armi KEE-Flag mutant
551 was produced by inverse PCR using RNAi-resistant Armi WT-Flag vector as a template.
552 The Flag-Luc expression vector was generated from pAc-Myc-Luc (a gift from H. Ishizu)
553 by substituting Myc with 3×Flag. The MOV10L1 and ASZ1 coding region was amplified
554 from total mouse ovary RNAs by RT-PCR and inserted into pAc-Armi WT-Flag and Myc-
555 Daed WT by substituting original coding regions. The primers used are shown in Table

556 S1.

557

558 **RNAi and transfection**

559 To initiate RNAi, 5.0×10^6 OSCs were mixed with 200 pmol of siRNAs in 20 μL of Solution
560 SF of the Cell Line Nucleofector Kit SF (Lonza Bioscience) and electroporation was
561 performed using a Nucleofector 96-well Shuttle device (Lonza Bioscience). For plasmid
562 transfection or plasmid/siRNA co-transfection, 1.5×10^7 OSCs were mixed with 1.5–10
563 μg of plasmids with or without 600 pmol of siRNAs in 100 μL of transfection buffer [180
564 mM sodium phosphate buffer for Church and Gilbert hybridization (pH 7.2), 5 mM KCl,
565 15 mM $MgCl_2$, and 50 mM D-mannitol] modified from a previous report,[86] and
566 electroporation was performed by a Nucleofector 2b device (Lonza Bioscience). Cells
567 were transfected with siRNAs twice with a 48-h interval. For rescue assays, endogenous
568 genes were depleted by RNAi and plasmids and siRNAs were introduced into the cells
569 after 48 h of culture. Cells were harvested after another 48 h of culture. For
570 immunofluorescence in Figure 2F, 500 pmol of siRNAs were used for RNAi and
571 plasmid/siRNA co-transfection, and cells were harvested after another 72 h of culture.
572 Sequences of siRNAs are indicated in Table S2.

573

574 **Production of anti-Daed monoclonal antibody**

575 GST-Daed (Met1–Asp197) was expressed in *E. coli* (Rosetta-DE3) and the inclusion
576 bodies were used for mouse immunization. Production and selection of hybridomas that
577 produce anti-Daed monoclonal antibodies were performed as described previously.[87]

578

579 **Mitochondrial fractionation**

580 Mitochondria were fractionated as previously reported.[12] Briefly, 1.2 × 10^8 OSCs were
581 suspended in 500 μL of buffer A [30 mM Tris-HCl (pH 7.3), 225 mM D-mannitol, 75 mM
582 sucrose, and 0.05 mM EGTA] and the cell suspension was passed 30 times through a
583 30-gauge needle attached to a 1-mL syringe. The lysates were centrifuged at 600 *g* for
584 5 min and the supernatants were collected, and repeated twice. The lysates were then
585 centrifuged at 7,000 *g* for 10 min and the supernatants were collected as the cytoplasmic
586 fraction. This step was also repeated twice. The pellets were resuspended in 500 μL of
587 buffer B [30 mM Tris-HCl (pH 7.3), 225 mM D-mannitol, and 75 mM sucrose] and
588 centrifuged at 10,000 *g* for 10 min. The supernatant was used as the mitochondrial
589 fraction.
590
591 **Nuclear fractionation**
592 Nuclear fractionation was performed as previously reported with some modifications. In
593 brief, cells were suspended in hypotonic buffer [10 mM HEPES-KOH (pH 7.3), 10 mM
594 KCl, 1.5 mM $MgCl_2$, 0.5 mM dithiothreitol (DTT), 2 μg/mL leupeptin, 2 μg/mL pepstatin
595 A, and 0.5% aprotinin] by pipetting six times and passed 3 times through a 25-gauge
596 needle attached to a 1-mL syringe. The lysates were centrifuged at 400 *g* for 10 min to
597 collect nuclei. The supernatants were collected as the cytoplasmic fraction, then the
598 concentration of KCl was adjusted to 200 mM and centrifuged at 20,000 *g* for 20 min
599 before used for Piwi-piRISC isolation (see below). The nuclear fraction was washed with
600 hypotonic buffer and resuspended in chromatin co-immunoprecipitation buffer [50 mM
601 HEPES-KOH (pH 7.3), 200 mM KCl, 1 mM EDTA, 1% Triton X-100, 0.1% Na
602 deoxycholate, 2 μg/mL leupeptin, 2 μg/mL pepstatin A, and 0.5% aprotinin]. The nuclear
603 fraction was sonicated and centrifuged at 20,000 *g* for 20 min. The supernatant was

604 collected as nuclear extract fraction for Piwi-piRISC isolation.

605

606 **Western blotting**

607 Western blotting was performed essentially as described previously.[88] Proteins
608 separated on SDS polyacrylamide gels were transferred to ClearTrans SP PVDF
609 membranes (Fujifilm Wako Pure Chemical) and incubated in PBS containing 0.1%
610 Tween-20 (T-PBS) supplemented with 5% skimmed milk. After washing with T-PBS, the
611 membranes were incubated with the following primary antibodies: anti-Daed (1:1,000
612 dilution, this study), anti-Gasz (1:1,000 dilution),[12] anti-Armi (2F8A9, 1:1,000 dilution),[16]
613 anti-Piwi (3G11, 1:1,000 dilution),[36] anti-β-Tub (1:1,000 dilution, E7, Developmental
614 Studies Hybridoma Bank), anti-HSP60(1:500 dilution, LK1, StressMarq Biosciences),
615 anti-Flag M2 (1:5,000 dilution, F3165, Sigma), anti-Histon H3 (1:5,000 dilution, ab1791,
616 abcam) monoclonal and anti-c-Myc (1:1,000 dilution, C3956, Sigma) polycronal
617 antibodies. After washing with T-PBS, the membranes were incubated with peroxidase-
618 conjugated anti-mouse IgG antibodies (1:5,000 dilution, 55558, Cappel) or anti-rabbit
619 IgG antibodies (1:5,000 dilution, 7074, Cell Signaling Technology). The membranes
620 were then reacted with Clarity Western ECL Substrate (Bio-Rad) and images were
621 collected using ChemiDoc XRS Plus System (Bio-Rad). The signal intensity was
622 quantified by Fiji (Ver. 2.0.0-rc-69/1.52p).[71]

623

624 **Immunofluorescence**

625 Immunofluorescence was performed as described previously.[16] OSCs were fixed with
626 4% formaldehyde in PBS. The cells were permeabilized with PBS containing 0.1% Triton
627 X-100, blocked with PBS containing 3% BSA, and incubated with the following primary

628 antibodies: anti-Armi (2F8A9, 1:200 dilution),[16] anti-Piwi (4D2, 1:200 dilution,[36] anti-Yb
629 (1G2H3, 1:200 dilution),[56] anti-Flag M2 (F3165, 1:1,000 dilution, Sigma) monoclonal and
630 anti-c-Myc (1:300 dilution, C3956, Sigma) polyclonal antibodies. Anti-Flag polyclonal
631 antibodies (F7425, 1:300 dilution, Sigma) were used to obtain the results shown in Figure
632 2F. After washing with PBS, cells were incubated with the following secondary antibodies
633 (1:1,000 dilution): Alexa 488-conjugated anti-mouse IgG1, Alexa 488-conjugated anti-
634 mouse IgG2b, Alexa 555-conjugated anti-mouse IgG1, Alexa 555-conjugated anti-
635 mouse IgG2b, Alexa 488-conjugated anti-rabbit IgG and Alexa 633-conjugated anti-
636 rabbit IgG (all from Thermo Fisher Scientific). Mitochondria were stained with
637 MitoTracker Orange CMXRos (Thermo Fisher Scientific) before fixation. Cells were
638 mounted with VECTASHIELD Mounting Medium with DAPI (Vector Laboratories).
639 Images were obtained using LSM980 laser scanning confocal microscope (Carl Zeiss).
640

641 **Immunoprecipitation**

642 Immunoprecipitation was performed as described previously.[16] Cells were suspended in
643 binding buffer A [30 mM HEPES-KOH (pH 7.3), 150 mM KOAc, 5 mM $Mg(OAc)_2$, 5 mM
644 DTT, 1% Triton X-100, 2 μg/mL leupeptin, 2 μg/mL pepstatin A, and 0.5% aprotinin]
645 supplemented with 0.04 U/μL RNasin Plus RNase Inhibitor (Promega) and the cell
646 suspension was passed 10 times through a 30-gauge needle and centrifuged. The
647 obtained supernatants (cell lysates) were incubated at 4°C with Dynabeads Protein G
648 (Thermo Fisher Scientific) pre-bound with antibodies. After 1 h of incubation, the beads
649 were washed with binding buffer and the materials bound on the beads were analyzed.
650

651 **Piwi-piRISC isolation from OSCs**

652 Cells were lysed by sonication in binding buffer B [50 mM HEPES-KOH (pH 7.3), 200
653 mM KCl, 1 mM EDTA, 1 mM DTT, 1% Triton X-100, 0.1% Na deoxycholate, 2 μg/mL
654 leupeptin, 2 μg/mL pepstatin A, and 0.5% aprotinin] supplemented with 0.1 U/μL RNasin
655 Plus RNase Inhibitor. Cell lysates were then incubated with anti-Piwi monoclonal
656 antibodies (3G11) pre-bound to Dynabeads Protein G at 4°C for 2 h. The beads were
657 washed with IP-wash buffer [20 mM HEPES-KOH (pH 7.3), 300 mM NaCl, 1 mM DTT,
658 0.05% NP-40, 2 μg/mL leupeptin, 2 μg/mL pepstatin A, and 0.5% aprotinin] and with
659 high-salt IP-wash buffer [20 mM HEPES-KOH (pH 7.3), 500 mM NaCl, 1 mM DTT, 0.05%
660 NP-40, 2 μg/mL leupeptin, 2 μg/mL pepstatin A, and 0.5% aprotinin]. RNAs were eluted
661 from the beads with phenol-chloroform and precipitated with ethanol. Eluted RNAs were
662 separated on denaturing polyacrylamide gels and detected by SYBR Gold Nucleic Acid
663 Gel Stain (Thermo Fisher Scientific). Signal intensity was calculated using Fiji, and
664 displayed using Python3 and seaborn (Ver.0.12.2). For piRNA sequencing, cells were
665 lysed in binding buffer C [20 mM HEPES-KOH (pH 7.3), 150 mM NaCl, 1mM EDTA, 1
666 mM DTT, 0.5% NP-40, 2 μg/mL leupeptin, 2 μg/mL pepstatin A, and 0.5% aprotinin]
667 supplemented with 0.04 U/μL RNasin Plus RNase Inhibitor. RNAs were separated on
668 denaturing polyacrylamide gels and 20–40-nt RNAs were eluted from the gels and
669 cloned as described previously.[8] QIAseq FastSelect-rRNA Fly Kit (QIAGEN) was used
670 to remove rRNA from the library.
671
672 **Northern blotting**
673 Total RNAs were isolated from OSCs using ISOGEN II (Fujifilm Wako Pure Chemical)
674 and treated with 0.04 U/μL TURBO DNase (Life Technologies). Northern blotting was
675 carried out as described previously.[89] Total RNAs were separated on denaturing

676 polyacrylamide gels, blotted on Hybond-N+ hybridization membranes (Cytiva), and UV
677 cross-linked. The membranes were incubated at 42°C for 30 min in hybridization buffer
678 [200 mM sodium phosphate buffer (pH 7.2), 7% SDS, and 1 mM EDTA] and probed with
679 ^{32}P-labeled oligonucleotides at 42°C overnight. The membranes were washed with NB-
680 wash buffer [30 mM sodium citrate (pH 7.0), 300 mM NaCl, and 0.1% SDS] at 42°C and
681 scanned using Typhoon FLA 9500 (Cytiva). Sequences of oligodeoxynucleotides are
682 shown in Table S3.
683
684 **RT-qPCR**
685 Total RNAs from OSCs were reverse-transcribed using ReverTra Ace (Toyobo).
686 Resulting cDNAs were amplified with StepOnePlus (Thermo Fisher Scientific) using
687 PowerUp SYBR Green Master Mix (Thermo Fisher Scientific). Sequences of primers are
688 shown in Table S4.
689
690 **Recombinant proteins**
691 GST-Daed ΔTM-His was expressed in *E. coli* (Rosetta DE3) at 16°C overnight. *E. coli*
692 was harvested and lysed by sonication in lysis buffer [30 mM Tris-HCl (pH 8.0), 500 mM
693 NaCl, 1% Triton X-100, 10 mM imidazole, 1× cOmplete ULTRA Tablets (Roche), and 1
694 mM DTT]. The supernatants after centrifugation were bound to Ni-Sepharose 6 Fast
695 Flow (Cytiva) at 4°C for 1 h. After washing with wash buffer A [30 mM Tris-HCl (pH 8.0),
696 500 mM NaCl, 1% Triton X-100, 10 mM imidazole, and 1 mM DTT], proteins were eluted
697 from the beads with elution buffer A [30 mM Tris-HCl (pH 8.0), 150 mM NaCl, 1% Triton
698 X-100, 250 mM imidazole, and 1 mM DTT]. Eluted proteins were bound to Glutathione
699 Sepharose 4B (Cytiva) at 4°C for 1 h. After washing with wash buffer B [30 mM Tris-HCl

700 (pH 8.0), 500 mM NaCl, 1% Triton X-100, and 1 mM DTT], proteins were eluted from the
701 beads with elution buffer B [30 mM Tris-HCl (pH 8.0), 150 mM NaCl, 1% Triton X-100, 1
702 mM DTT, and 15 mM glutathione], dialyzed in dialysis buffer [30 mM Tris-HCl (pH 8.0),
703 150 mM NaCl, 1 mM DTT, 10% glycerol, and 8 μg/mL GST-HRV3C protease], and
704 passed through Glutathione Sepharose 4B to remove the protease and GST.
705
706 **Pull-down assay**
707 OSCs expressing Armi WT-Flag and its ΔN34 mutant were suspended with bait-
708 preparing buffer [30 mM HEPES-KOH (pH 7.3), 150 mM KOAc, 500 mM NaCl, 5 mM
709 $Mg(OAc)_2$, 5 mM DTT, 1% Triton X-100, 2 μg/mL leupeptin, 2 μg/mL pepstatin A, 0.5%
710 aprotinin, and 25 μg/mL RNase A (Roche)]. The cell suspension was passed five times
711 through a 25-gauge needle and another five times through a 30-gauge needle, and then
712 centrifuged. The supernatants were incubated at 4°C for 1 h with anti-Flag antibodies
713 pre-bound onto Dynabeads Protein G. Beads were washed with bait-preparing buffer
714 and then binding buffer D [30 mM Tris-HCl (pH 8.0), 150 mM NaCl, 1 mM DTT, and 1%
715 Triton X-100]. Daed ΔTM-His was added to the beads and incubated at 4°C for 1.5 h.
716 After washing with binding buffer, proteins were eluted from the beads, separated on an
717 SDS polyacrylamide gel, and stained with CBB.
718
719 **β-elimination assay**
720 β-elimination was performed as described previously with some modifications.[37] piRNAs
721 were isolated from Piwi immunoprecipitated from OSCs. miRNAs were isolated from
722 Ago1 immunoprecipitated from OSCs using monoclonal anti-Ago1 antibodies[57]. RNAs
723 were incubated in 10 mM $NaIO_4$ for 40 min at 0°C in the dark. After ethanol precipitation,

724 RNAs were dissolved in 1 M L(+)-lysine-HCl (pH 8.5) and incubated for 90 min at 45°C.
725 After ethanol precipitation, RNAs were separated on a denaturing polyacrylamide gel
726 and detected by SYBR Gold Nucleic Acid Gel Stain.
727
728 **piRNA sequencing and bioinformatic analysis**
729 piRNAs were sequenced using MiSeq (Illumina) with MiSeq Reagent Kit v3 (Illumina).
730 piRNA-seq analysis was performed as described previously[8] with some modifications.
731 Adapter-trimmed reads of ≥ 18 nt in length were mapped against the *Drosophila* genome
732 (BDGP Release 6 + ISO1 MT/dm6) with FlyBase gene model (Release 6.21) using
733 STAR[64] (Ver. 2.7.8a). Uniquely mapped reads with up to one mismatch were used for
734 the subsequent analysis. Read length of each biological triplicate was used in the
735 analysis in Figures 4B and S6A. After confirming high correlations between samples
736 (Figures S9A and S9B), reads were merged and used for subsequent analysis. Reads
737 mapped to exons of coding genes (Figures S9A and S9B) were counted with HTSeq[65]
738 (Ver. 0.9.1) using annotation file obtained from FlyBase and normalized to RPM+1 reads.
739 Spearman's rho was calculated using R[62] (Ver. 4.3.1). For transposon annotation
740 (Figures S4B and S4C), the annotation file of repeat sequences was obtained from
741 RepeatMasker (dm6-Apr 2006-RepeatMasker open-4.0.6-Dfam 2.0) and transposons
742 were extracted without distinction between int and LTR. Reads mapped antisense to
743 transposons were counted using HTSeq. For the analysis in Figure S4C, reads were
744 normalized to RPM+1 reads. For the analysis in Figure S4B, transposons which mapped
745 > 5 RPM reads in the sum of WT and ΔSAM were selected, and the mean length of
746 mapped reads for each transposon were calculated. For 1U bias and +1U bias analyses
747 (Figures 4C, 4I, and S6B), the 5′ ends and their downstream sequences of piRNAs (1U

748 bias) or *Drosophila* genome sequences around the 3′ ends (+1U bias) were obtained
749 using bedtools[66] (Ver. 2.30.0) and SAMtools (Ver. 1.9).[67] Sequence logos were
750 generated using ggseqlogo.[69] For the phasing analysis (Figure 4D), 3′ end positions
751 around piRNA 5′ end position were normalized to RPM and showed in heatmaps using
752 RSeQC[70] (Ver. 2.6.4), deepTools[68] (Ver. 3.3.2), SAMtools[67] (Ver. 1.9) and "wigToBigWig"
753 from UCSC. Binary histograms were generated using the matrix of heatmaps. Values
754 were transformed into binary format (counts = 0 → 0, counts > 0 → 1) in accordance
755 with a previous study.[18] For the comparison of 3′ end position in WT and mutant libraries
756 of Daed or Armi (Figures 4H and S6C), 50,000 piRNA 5′ end positions, common to the
757 WT and mutant libraries and most abundant in the WT library, were extracted. The
758 percentage of 3′ end positions corresponding to each 5′ end position was calculated and
759 shown in heatmaps. 5′ end positions were ordered by the 3′ end position of WT library
760 data and the same order was maintained in the mutant library data. In Figure S4G, the
761 length of dominant piRNAs produced from the 5′ end was used for the 5′-end clarification.
762 First, the 5′ end positions that dominantly produce 26- or 27-nt piRNAs in the WT library
763 was extracted, and after combining, these positions were classified as "Unchanged" and
764 "Elongated" according to the length of dominant piRNAs in ΔSAM library. The
765 subsequent analysis was conducted using the piRNAs produced from each 5′-end
766 groups.
767
768 **piRISC production simulation**
769 The *flam* sequence was downloaded from FlyBase (Release FB2023_05) (21,629,891
770 to 21,792,731 on the X chromosome) and subjected to the digestion into 163 piRNA
771 precursors (starting at U and around 1,000 nt). The precursors were cleaved to 18–40-

772 nt piRNAs immediately before U. The cleavage position was determined based on the
773 distribution of the actual piRNA length, which was obtained by fitting a normal distribution
774 to the piRNA sequencing data. The simulation was performed using Python3[58] (Ver.
775 3.8.8) with add-on libraries [Numpy[59] (Ver. 1.20.1), Scipy[60] (Ver. 1.6.2), and Pandas[61]
776 (Ver. 1.2.4)].
777
778 **Structure prediction**
779 A structure model of the AmTEC (Figure 1A) and Armi–AmTEC complex (Figure 3A) was
780 built by structure prediction with ColabFold[90] (Ver. 1.5.5) and AlphaFold[32] (Ver. 2.3) using
781 protein amino acid sequences from FlyBase (Release FB2023_04). Five complex
782 models were built, and structural predictions and optimization were performed five times
783 for each complex model. The structure model with the highest pLDDT value underwent
784 relax steps. The N-terminal disorder region and TM domain orientations of Daed and
785 Gasz were appropriately changed at the linker region using ISOLDE[74] (Ver. 1.6). The
786 structure was visualized using UCSF ChimeraX[73] (Ver. 1.6.1).
787
788 **Molecular dynamics simulation**
789 The protein complex was embedded in a bilayer membrane in the simulation box
790 described below using CHARMM-GUI Martini bilayer maker[75–77] (Ver. 3.8). Orientation
791 of the protein complex in lipid bilayer was determined using PPM 3.0 Web Server[78] prior
792 to the construction of the simulation box. The structure model of the Armi–AmTEC [Daed
793 (ΔSAM)] complex was generated using PyMOL (2.5.0), UCSF ChimeraX, and ISOLDE
794 based on the Armi–AmTEC complex model. Initial structures were arranged in the
795 250×250 nm bilayer membrane (67% of POPC and 33% DOPE, containing roughly

796 2,000 lipid molecules in total) and the thickness of water at the top and bottom of the
797 system was set to 100 nm. Ionic strength and temperature were set to 150 mM NaCl and
798 303.15 K, respectively. Molecular dynamics simulations were performed using
799 GROMACS[79] (Version 2021.2) with Martini 3 coarse-grained model.[91] First, energy
800 minimization was performed using the steepest-descent method. Then, equilibration was
801 conducted using the V-rescale method five times (2 fs×500,000 steps, 5 fs×200,000
802 steps, 10 fs×100,000 steps, 15 fs×50,000 steps, and 20 fs×50,000 steps). After the
803 equilibration runs, simulations were performed at 20 fs for 50,000,000 steps. The
804 structural trajectories were calculated using gmx trjconv tool for clustering and centering
805 of the protein complex. The root mean square deviation (RMSD) of protein complexes
806 were calculated using gmx rms tool. The distances between the center of mass of Armi
807 helicase domain (Ser697–Cys1,148) and that of AmTEC were calculated using Python3
808 (Ver. 3.9.18) with add-on libraries [Numpy (Ver. 1.24.3) and MDAnalysis[80,81] (Ver. 2.7.0)],
809 and visualized using R.[62]

810

811 **Ortholog search and protein sequence alignment**

812 Orthologs for Armi/MOV10L1, Gasz/ASZ1, PNLDC1, Papi/TDRKH, Nbr were searched
813 using OrthoDB v11. Orthologs for Daed were searched using OrthoDB v11[39] and NCBI
814 PSI-Blast. Species taxonomy was according to NCBI and phylogenetic tree (Figure 5A)
815 were generated following previous studies.[92,93] Multiple sequence alignment (Figure
816 S5B) was conducted using CLUSTAL Omega multiple alignment[82] and visualized using
817 ESPript (Ver. 3.0).[84] The phylogenetic tree (Figure S5A) was generated using Neighbor-
818 Joining method[94] in MEGA11[85]. Multiple sequence alignment (Figure S6) was

819 conducted using CLUSTAL Omega multiple alignment[82] and visualized using iTOL (Ver.
820 6.9)[83]. The following protein sequences were acquired from NCBI: *D. melanogaster* Armi
821 (NP_001014556), *H. sapiens* Moloney leukemia virus 10-like protein 1 (MOV10L1)
822 (NP_061868.1), *M. musculus* MOV10L1 (XP_006521619.1), *G. gallus* MOV10L1
823 (XP_040514825.1), *X. tropicalis* MOV10L1 (NP_001072624.1), *D. rerio* MOV10L1
824 (NP_001070795.1), *Z. nevadensis* Armi (XP_021937793.1), *T. palmi* Armi
825 (XP_034251738.1), *A. echinatior* Armi (XP_011062616.1), *B. terrestris* Armi
826 (XP_012166280.1), *D. ponderosae* Armi (XP_048525683.1), *T. castaneum* Armi
827 (XP_008199251.1), *B. anynana* Armi (XP_023946786.2), *B. mori* Armi
828 (XP_037867032.1), *A. gambiae* Armi (XP_061506580.1), *A. aegypti* Armi
829 (XP_021698921.1), *B. dorsalis* Armi (XP_011214121.1), *C. capitata* Armi
830 (XP_004537921.1), *M. domestica* Armi (XP_058975516.1) and *S. calcitrans* Armi
831 (XP_013110641.2).

832

833 **Quantification and statistical analysis**

834 All experiments were performed over two independent experiments (biological
835 replicates). Sample sizes were predetermined following previously performed
836 experiments with similar setup in the field. Statistical methods, *p* value and number of
837 replicates are indicated in each figure and its legend. Statistical analyses were performed
838 in the R software environment (version 4.3.1). Shapiro-Wilk test was used for testing
839 normality when statistical methods based on the normal distribution was used.
840 Experiments were not blinded as consistent with the previous studies in the field.

841

842 **Supplemental information**

843 Document S1. Figures S1–S9 and Table S1–S4

844

845 **Supplemental figure titles**

846 Figure S1. Related to Figure 1; Coiled-coil prediction and specificity of anti-Daed
847 antibodies

848 Figure S2. Related to Figure 2; Functions and behaviors of Daed and Gasz in OSCs

849 Figure S3. Related to Figure 3; Effects of Armi mutants on piRNA biogenesis

850 Figure S4. Related to Figure 4; Effects of Daed ΔSAM on piRNA biogenesis and Piwi-
851 piRISC function

852 Figure S5. Related to Figure 4; MD simulation of Armi–AmTEC complex

853 Figure S6. Related to Figure 4; Effects of Armi KEE on piRNA biogenesis

854 Figure S7. Related to Figure 5; Sequence alignment of Daed in species

855 Figure S8. Related to Figure 5; Sequence alignment of Armi UPF1-like helicase domain
856 in species

857 Figure S9. Related to STAR Method "piRNA sequencing and bioinformatic analysis";
858 Reproducibility of piRNA-seq

859

860 **Supplemental table titles**

861 Table S1. Related to STAR Method "Plasmid construction"; Sequences of primers used
862 for plasmid construction

863 Table S2. Related to STAR Method "RNAi and transfection"; Sequences of siRNAs

864 Table S3. Related to STAR Method "Northern blotting"; Sequences of oligos used for
865 northern blotting

866 Table S4. Related to STAR Method "RT-qPCR"; Sequences of primers used for RT-

867 qPCR

868

869 **References**

870 1. Czech, B., Munafò, M., Ciabrelli, F., Eastwood, E.L., Fabry, M.H., Kneuss, E., and
871 Hannon, G.J. (2018). piRNA-Guided Genome Defense: From Biogenesis to
872 Silencing. Annual Review of Genetics *52*, 131–157.
873 https://doi.org/10.1146/annurev-genet-120417-031441.
874 2. Huang, X., Fejes Tóth, K., and Aravin, A.A. (2017). piRNA Biogenesis in Drosophila
875 melanogaster. Trends in Genetics *33*, 882–894.
876 https://doi.org/10.1016/j.tig.2017.09.002.
877 3. Ozata, D.M., Gainetdinov, I., Zoch, A., O'Carroll, D., and Zamore, P.D. (2019). PIWI-
878 interacting RNAs: small RNAs with big functions. Nat Rev Genet *20*, 89–108.
879 https://doi.org/10.1038/s41576-018-0073-3.
880 4. Yamashiro, H., and Siomi, M.C. (2018). PIWI-Interacting RNA in Drosophila:
881 Biogenesis, Transposon Regulation, and Beyond. Chem Rev *118*, 4404–4421.
882 https://doi.org/10.1021/acs.chemrev.7b00393.
883 5. Brennecke, J., Aravin, A.A., Stark, A., Dus, M., Kellis, M., Sachidanandam, R., and
884 Hannon, G.J. (2007). Discrete Small RNA-Generating Loci as Master Regulators of
885 Transposon Activity in Drosophila. Cell *128*, 1089–1103.
886 https://doi.org/10.1016/j.cell.2007.01.043.
887 6. Malone, C.D., Brennecke, J., Dus, M., Stark, A., McCombie, W.R., Sachidanandam,
888 R., and Hannon, G.J. (2009). Specialized piRNA Pathways Act in Germline and
889 Somatic Tissues of the Drosophila Ovary. Cell *137*, 522–535.
890 https://doi.org/10.1016/j.cell.2009.03.040.
891 7. Goriaux, C., Desset, S., Renaud, Y., Vaury, C., and Brasset, E. (2014).
892 Transcriptional properties and splicing of the flamenco piRNA cluster. EMBO reports
893 *15*, 411–418. https://doi.org/10.1002/embr.201337898.
894 8. Hirakata, S., Ishizu, H., Fujita, A., Tomoe, Y., and Siomi, M.C. (2019). Requirements
895 for multivalent Yb body assembly in transposon silencing in Drosophila. EMBO Rep
896 *20*, e47708. https://doi.org/10.15252/embr.201947708.
897 9. Ishizu, H., Iwasaki, Y.W., Hirakata, S., Ozaki, H., Iwasaki, W., Siomi, H., and Siomi,
898 M.C. (2015). Somatic Primary piRNA Biogenesis Driven by cis-Acting RNA
899 Elements and trans-Acting Yb. Cell Reports *12*, 429–440.
900 https://doi.org/10.1016/j.celrep.2015.06.035.
901 10. Cora, E., Pandey, R.R., Xiol, J., Taylor, J., Sachidanandam, R., McCarthy, A.A., and

Pillai, R.S. (2014). The MID-PIWI module of Piwi proteins specifies nucleotide- and strand-biases of piRNAs. RNA *20*, 773–781. https://doi.org/10.1261/rna.044701.114.

11. Stein, C.B., Genzor, P., Mitra, S., Elchert, A.R., Ipsaro, J.J., Benner, L., Sobti, S., Su, Y., Hammell, M., Joshua-Tor, L., et al. (2019). Decoding the 5′ nucleotide bias of PIWI-interacting RNAs. Nat Commun *10*, 828. https://doi.org/10.1038/s41467-019-08803-z.
12. Yamashiro, H., Negishi, M., Kinoshita, T., Ishizu, H., Ohtani, H., and Siomi, M.C. (2020). Armitage determines Piwi–piRISC processing from precursor formation and quality control to inter-organelle translocation. EMBO reports *21*, e48769. https://doi.org/10.15252/embr.201948769.
13. Choi, S.-Y., Huang, P., Jenkins, G.M., Chan, D.C., Schiller, J., and Frohman, M.A. (2006). A common lipid links Mfn-mediated mitochondrial fusion and SNARE-regulated exocytosis. Nat Cell Biol *8*, 1255–1262. https://doi.org/10.1038/ncb1487.
14. Ipsaro, J.J., Haase, A.D., Knott, S.R., Joshua-Tor, L., and Hannon, G.J. (2012). The structural biochemistry of Zucchini implicates it as a nuclease in piRNA biogenesis. Nature *491*, 279–283. https://doi.org/10.1038/nature11502.
15. Nishimasu, H., Ishizu, H., Saito, K., Fukuhara, S., Kamatani, M.K., Bonnefond, L., Matsumoto, N., Nishizawa, T., Nakanaga, K., Aoki, J., et al. (2012). Structure and function of Zucchini endoribonuclease in piRNA biogenesis. Nature *491*, 284–287. https://doi.org/10.1038/nature11509.
16. Saito, K., Ishizu, H., Komai, M., Kotani, H., Kawamura, Y., Nishida, K.M., Siomi, H., and Siomi, M.C. (2010). Roles for the Yb body components Armitage and Yb in primary piRNA biogenesis in Drosophila. Genes Dev *24*, 2493–2498. https://doi.org/10.1101/gad.1989510.
17. Han, B.W., Wang, W., Li, C., Weng, Z., and Zamore, P.D. (2015). Noncoding RNA. piRNA-guided transposon cleavage initiates Zucchini-dependent, phased piRNA production. Science *348*, 817–821. https://doi.org/10.1126/science.aaa1264.
18. Mohn, F., Handler, D., and Brennecke, J. (2015). piRNA-guided slicing specifies transcripts for Zucchini-dependent, phased piRNA biogenesis. Science *348*, 812–817. https://doi.org/10.1126/science.aaa1039.
19. Yashiro, R., Murota, Y., Nishida, K.M., Yamashiro, H., Fujii, K., Ogai, A., Yamanaka, S., Negishi, L., Siomi, H., and Siomi, M.C. (2018). Piwi Nuclear Localization and Its Regulatory Mechanism in Drosophila Ovarian Somatic Cells. Cell Reports *23*, 3647–3657. https://doi.org/10.1016/j.celrep.2018.05.051.
20. Dönertas, D., Sienski, G., and Brennecke, J. (2013). Drosophila Gtsf1 is an essential component of the Piwi-mediated transcriptional silencing complex. Genes Dev *27*,

938 1693–1705. https://doi.org/10.1101/gad.221150.113.
939 21. Fabry, M.H., Ciabrelli, F., Munafò, M., Eastwood, E.L., Kneuss, E., Falciatori, I.,
940 Falconio, F.A., Hannon, G.J., and Czech, B. (2019). piRNA-guided co-transcriptional
941 silencing coopts nuclear export factors. eLife *8*, e47999.
942 https://doi.org/10.7554/eLife.47999.
943 22. Murano, K., Iwasaki, Y.W., Ishizu, H., Mashiko, A., Shibuya, A., Kondo, S., Adachi,
944 S., Suzuki, S., Saito, K., Natsume, T., et al. (2019). Nuclear RNA export factor
945 variant initiates piRNA-guided co-transcriptional silencing. The EMBO Journal *38*,
946 e102870. https://doi.org/10.15252/embj.2019102870.
947 23. Ohtani, H., Iwasaki, Y.W., Shibuya, A., Siomi, H., Siomi, M.C., and Saito, K. (2013).
948 DmGTSF1 is necessary for Piwi–piRISC-mediated transcriptional transposon
949 silencing in the Drosophila ovary. Genes Dev *27*, 1656–1661.
950 https://doi.org/10.1101/gad.221515.113.
951 24. Onishi, R., Sato, K., Murano, K., Negishi, L., Siomi, H., and Siomi, M.C. (2020). Piwi
952 suppresses transcription of Brahma-dependent transposons via Maelstrom in
953 ovarian somatic cells. Science Advances *6*, eaaz7420.
954 https://doi.org/10.1126/sciadv.aaz7420.
955 25. Sienski, G., Dönertas, D., and Brennecke, J. (2012). Transcriptional silencing of
956 transposons by Piwi and maelstrom and its impact on chromatin state and gene
957 expression. Cell *151*, 964–980. https://doi.org/10.1016/j.cell.2012.10.040.
958 26. Sienski, G., Batki, J., Senti, K.-A., Dönertas, D., Tirian, L., Meixner, K., and
959 Brennecke, J. (2015). Silencio/CG9754 connects the Piwi–piRNA complex to the
960 cellular heterochromatin machinery. Genes Dev *29*, 2258–2271.
961 https://doi.org/10.1101/gad.271908.115.
962 27. Yu, Y., Gu, J., Jin, Y., Luo, Y., Preall, J.B., Ma, J., Czech, B., and Hannon, G.J.
963 (2015). Panoramix enforces piRNA-dependent cotranscriptional silencing. Science
964 *350*, 339–342. https://doi.org/10.1126/science.aab0700.
965 28. Czech, B., Preall, J.B., McGinn, J., and Hannon, G.J. (2013). A transcriptome-wide
966 RNAi screen in the Drosophila ovary reveals factors of the germline piRNA pathway.
967 Mol Cell *50*, 749–761. https://doi.org/10.1016/j.molcel.2013.04.007.
968 29. Munafò, M., Manelli, V., Falconio, F.A., Sawle, A., Kneuss, E., Eastwood, E.L., Seah,
969 J.W.E., Czech, B., and Hannon, G.J. (2019). Daedalus and Gasz recruit Armitage
970 to mitochondria, bringing piRNA precursors to the biogenesis machinery. Genes Dev.
971 *33*, 844–856. https://doi.org/10.1101/gad.325662.119.
972 30. Ge, D.T., Wang, W., Tipping, C., Gainetdinov, I., Weng, Z., and Zamore, P.D. (2019).
973 The RNA-Binding ATPase, Armitage, Couples piRNA Amplification in Nuage to

Phased piRNA Production on Mitochondria. Molecular Cell *74*, 982-995.e6. https://doi.org/10.1016/j.molcel.2019.04.006.

31. Evans, R., O'Neill, M., Pritzel, A., Antropova, N., Senior, A., Green, T., Žídek, A., Bates, R., Blackwell, S., Yim, J., et al. (2022). Protein complex prediction with AlphaFold-Multimer. Preprint at bioRxiv, https://doi.org/10.1101/2021.10.04.463034 https://doi.org/10.1101/2021.10.04.463034.
32. Jumper, J., Evans, R., Pritzel, A., Green, T., Figurnov, M., Ronneberger, O., Tunyasuvunakool, K., Bates, R., Žídek, A., Potapenko, A., et al. (2021). Highly accurate protein structure prediction with AlphaFold. Nature *596*, 583–589. https://doi.org/10.1038/s41586-021-03819-2.
33. Madeo, G., Savojardo, C., Manfredi, M., Martelli, P.L., and Casadio, R. (2023). CoCoNat: a novel method based on deep learning for coiled-coil prediction. Bioinformatics *39*, btad495. https://doi.org/10.1093/bioinformatics/btad495.
34. Saito, K., Inagaki, S., Mituyama, T., Kawamura, Y., Ono, Y., Sakota, E., Kotani, H., Asai, K., Siomi, H., and Siomi, M.C. (2009). A regulatory circuit for piwi by the large Maf gene traffic jam in Drosophila. Nature *461*, 1296–1299. https://doi.org/10.1038/nature08501.
35. Olivieri, D., Sykora, M.M., Sachidanandam, R., Mechtler, K., and Brennecke, J. (2010). An in vivo RNAi assay identifies major genetic and cellular requirements for primary piRNA biogenesis in Drosophila. EMBO J *29*, 3301–3317. https://doi.org/10.1038/emboj.2010.212.
36. Saito, K., Nishida, K.M., Mori, T., Kawamura, Y., Miyoshi, K., Nagami, T., Siomi, H., and Siomi, M.C. (2006). Specific association of Piwi with rasiRNAs derived from retrotransposon and heterochromatic regions in the Drosophila genome. Genes Dev *20*, 2214–2222. https://doi.org/10.1101/gad.1454806.
37. Gunawardane, L.S., Saito, K., Nishida, K.M., Miyoshi, K., Kawamura, Y., Nagami, T., Siomi, H., and Siomi, M.C. (2007). A Slicer-Mediated Mechanism for Repeat-Associated siRNA 5' End Formation in Drosophila. Science *315*, 1587–1590. https://doi.org/10.1126/science.1140494.
38. Horwich, M.D., Li, C., Matranga, C., Vagin, V., Farley, G., Wang, P., and Zamore, P.D. (2007). The Drosophila RNA Methyltransferase, DmHen1, Modifies Germline piRNAs and Single-Stranded siRNAs in RISC. Current Biology *17*, 1265–1272. https://doi.org/10.1016/j.cub.2007.06.030.
39. Kuznetsov, D., Tegenfeldt, F., Manni, M., Seppey, M., Berkeley, M., Kriventseva, E.V., and Zdobnov, E.M. (2023). OrthoDB v11: annotation of orthologs in the widest sampling of organismal diversity. Nucleic Acids Research *51*, D445–D451.

1010 https://doi.org/10.1093/nar/gkac998.
1011 40. Vourekas, A., Zheng, K., Fu, Q., Maragkakis, M., Alexiou, P., Ma, J., Pillai, R.S.,
1012 Mourelatos, Z., and Wang, P.J. (2015). The RNA helicase MOV10L1 binds piRNA
1013 precursors to initiate piRNA processing. Genes Dev *29*, 617–629.
1014 https://doi.org/10.1101/gad.254631.114.
1015 41. Zheng, K., Xiol, J., Reuter, M., Eckardt, S., Leu, N.A., McLaughlin, K.J., Stark, A.,
1016 Sachidanandam, R., Pillai, R.S., and Wang, P.J. (2010). Mouse MOV10L1
1017 associates with Piwi proteins and is an essential component of the Piwi-interacting
1018 RNA (piRNA) pathway. Proceedings of the National Academy of Sciences *107*,
1019 11841–11846. https://doi.org/10.1073/pnas.1003953107.
1020 42. Ikeda, S., Tanaka, K., Ohtani, R., Kanda, A., Sotomaru, Y., Kono, T., and Obata, Y.
1021 (2022). Disruption of piRNA machinery by deletion of ASZ1/GASZ results in the
1022 expression of aberrant chimeric transcripts in gonocytes. Journal of Reproduction
1023 and Development *68*, 125–136. https://doi.org/10.1262/jrd.2021-146.
1024 43. Ding, D., Liu, J., Dong, K., Midic, U., Hess, R.A., Xie, H., Demireva, E.Y., and Chen,
1025 C. (2017). PNLDC1 is essential for piRNA 3′ end trimming and transposon silencing
1026 during spermatogenesis in mice. Nat Commun *8*, 819.
1027 https://doi.org/10.1038/s41467-017-00854-4.
1028 44. Nishimura, T., Nagamori, I., Nakatani, T., Izumi, N., Tomari, Y., Kuramochi-
1029 Miyagawa, S., and Nakano, T. (2018). PNLDC1, mouse pre-piRNA Trimmer, is
1030 required for meiotic and post-meiotic male germ cell development. EMBO reports
1031 *19*, e44957. https://doi.org/10.15252/embr.201744957.
1032 45. Hayashi, R., Schnabl, J., Handler, D., Mohn, F., Ameres, S.L., and Brennecke, J.
1033 (2016). Genetic and mechanistic diversity of piRNA 3' end formation. Nature *539*,
1034 588–592. https://doi.org/10.1038/nature20162.
1035 46. Honda, S., Kirino, Y., Maragkakis, M., Alexiou, P., Ohtaki, A., Murali, R., Mourelatos,
1036 Z., and Kirino, Y. (2013). Mitochondrial protein BmPAPI modulates the length of
1037 mature piRNAs. RNA *19*, 1405–1418. https://doi.org/10.1261/rna.040428.113.
1038 47. Saxe, J.P., Chen, M., Zhao, H., and Lin, H. (2013). Tdrkh is essential for
1039 spermatogenesis and participates in primary piRNA biogenesis in the germline. The
1040 EMBO Journal *32*, 1869–1885. https://doi.org/10.1038/emboj.2013.121.
1041 48. Feltzin, V.L., Khaladkar, M., Abe, M., Parisi, M., Hendriks, G.-J., Kim, J., and Bonini,
1042 N.M. (2015). The exonuclease Nibbler regulates age-associated traits and
1043 modulates piRNA length in Drosophila. Aging Cell *14*, 443–452.
1044 https://doi.org/10.1111/acel.12323.
1045 49. Joosten, J., Overheul, G.J., Van Rij, R.P., and Miesen, P. (2021). Endogenous

1046 piRNA-guided slicing triggers responder and trailer piRNA production from viral RNA
1047 in Aedes aegypti mosquitoes. Nucleic Acids Research *49*, 8886–8899.
1048 https://doi.org/10.1093/nar/gkab640.
1049 50. Wang, H., Ma, Z., Niu, K., Xiao, Y., Wu, X., Pan, C., Zhao, Y., Wang, K., Zhang, Y.,
1050 and Liu, N. (2016). Antagonistic roles of Nibbler and Hen1 in modulating piRNA 3′
1051 ends in Drosophila. Development *143*, 530–539. https://doi.org/10.1242/dev.128116.
1052 51. Ishizu, H., Kinoshita, T., Hirakata, S., Komatsuzaki, C., and Siomi, M.C. (2019).
1053 Distinct and Collaborative Functions of Yb and Armitage in Transposon-Targeting
1054 piRNA Biogenesis. Cell Reports *27*, 1822-1835.e8.
1055 https://doi.org/10.1016/j.celrep.2019.04.029.
1056 52. Lee, Y.C.G., and Langley, C.H. (2012). Long-Term and Short-Term Evolutionary
1057 Impacts of Transposable Elements on Drosophila. Genetics *192*, 1411–1432.
1058 https://doi.org/10.1534/genetics.112.145714.
1059 53. Obbard, D.J., Gordon, K.H.J., Buck, A.H., and Jiggins, F.M. (2008). The evolution
1060 of RNAi as a defence against viruses and transposable elements. Philosophical
1061 Transactions of the Royal Society B: Biological Sciences *364*, 99–115.
1062 https://doi.org/10.1098/rstb.2008.0168.
1063 54. Parhad, S.S., and Theurkauf, W.E. (2019). Rapid evolution and conserved function
1064 of the piRNA pathway. Open Biology *9*, 180181.
1065 https://doi.org/10.1098/rsob.180181.
1066 55. Gamez, S., Srivastav, S., Akbari, O.S., and Lau, N.C. (2020). Diverse Defenses: A
1067 Perspective Comparing Dipteran Piwi-piRNA Pathways. Cells *9*, 2180.
1068 https://doi.org/10.3390/cells9102180.
1069 56. Murota, Y., Ishizu, H., Nakagawa, S., Iwasaki, Y.W., Shibata, S., Kamatani, M.K.,
1070 Saito, K., Okano, H., Siomi, H., and Siomi, M.C. (2014). Yb integrates piRNA
1071 intermediates and processing factors into perinuclear bodies to enhance piRISC
1072 assembly. Cell Rep *8*, 103–113. https://doi.org/10.1016/j.celrep.2014.05.043.
1073 57. Okamura, K., Ishizuka, A., Siomi, H., and Siomi, M.C. (2004). Distinct roles for
1074 Argonaute proteins in small RNA-directed RNA cleavage pathways. Genes Dev *18*,
1075 1655–1666. https://doi.org/10.1101/gad.1210204.
1076 58. Van Rossum, G., and Drake, F.L. (2009). Python 3 Reference Manual
1077 (CreateSpace).
1078 59. Harris, C.R., Millman, K.J., van der Walt, S.J., Gommers, R., Virtanen, P.,
1079 Cournapeau, D., Wieser, E., Taylor, J., Berg, S., Smith, N.J., et al. (2020). Array
1080 programming with NumPy. Nature *585*, 357–362. https://doi.org/10.1038/s41586-
1081 020-2649-2.

60. Virtanen, P., Gommers, R., Oliphant, T.E., Haberland, M., Reddy, T., Cournapeau, D., Burovski, E., Peterson, P., Weckesser, W., Bright, J., et al. (2020). SciPy 1.0: fundamental algorithms for scientific computing in Python. Nat Methods *17*, 261–272. https://doi.org/10.1038/s41592-019-0686-2.
61. McKinney, W. (2010). Data Structures for Statistical Computing in Python. Proceedings of the 9th Python in Science Conference, 56–61. https://doi.org/10.25080/Majora-92bf1922-00a.
62. R Development Core Team (2023). R : A language and environment for statistical computing. R Foundation for Statistical Computing, Vienna, Austria.
63. Martin, M. (2011). Cutadapt removes adapter sequences from high-throughput sequencing reads. EMBnet.journal *17*, 10–12. https://doi.org/10.14806/ej.17.1.200.
64. Dobin, A., Davis, C.A., Schlesinger, F., Drenkow, J., Zaleski, C., Jha, S., Batut, P., Chaisson, M., and Gingeras, T.R. (2013). STAR: ultrafast universal RNA-seq aligner. Bioinformatics *29*, 15–21. https://doi.org/10.1093/bioinformatics/bts635.
65. Anders, S., Pyl, P.T., and Huber, W. (2015). HTSeq--a Python framework to work with high-throughput sequencing data. Bioinformatics *31*, 166–169. https://doi.org/10.1093/bioinformatics/btu638.
66. Quinlan, A.R., and Hall, I.M. (2010). BEDTools: a flexible suite of utilities for comparing genomic features. Bioinformatics *26*, 841–842. https://doi.org/10.1093/bioinformatics/btq033.
67. Li, H., Handsaker, B., Wysoker, A., Fennell, T., Ruan, J., Homer, N., Marth, G., Abecasis, G., Durbin, R., and 1000 Genome Project Data Processing Subgroup (2009). The Sequence Alignment/Map format and SAMtools. Bioinformatics *25*, 2078–2079. https://doi.org/10.1093/bioinformatics/btp352.
68. Ramírez, F., Ryan, D.P., Grüning, B., Bhardwaj, V., Kilpert, F., Richter, A.S., Heyne, S., Dündar, F., and Manke, T. (2016). deepTools2: a next generation web server for deep-sequencing data analysis. Nucleic Acids Res *44*, W160-165. https://doi.org/10.1093/nar/gkw257.
69. Wagih, O. (2017). ggseqlogo: a versatile R package for drawing sequence logos. Bioinformatics *33*, 3645–3647. https://doi.org/10.1093/bioinformatics/btx469.
70. Wang, L., Wang, S., and Li, W. (2012). RSeQC: quality control of RNA-seq experiments. Bioinformatics *28*, 2184–2185. https://doi.org/10.1093/bioinformatics/bts356.
71. Schindelin, J., Arganda-Carreras, I., Frise, E., Kaynig, V., Longair, M., Pietzsch, T., Preibisch, S., Rueden, C., Saalfeld, S., Schmid, B., et al. (2012). Fiji: an open-source platform for biological-image analysis. Nat Methods *9*, 676–682.

https://doi.org/10.1038/nmeth.2019.

72. Waskom, M.L. (2021). seaborn: statistical data visualization. Journal of Open Source Software *6*, 3021. https://doi.org/10.21105/joss.03021.
73. Pettersen, E.F., Goddard, T.D., Huang, C.C., Meng, E.C., Couch, G.S., Croll, T.I., Morris, J.H., and Ferrin, T.E. (2021). UCSF ChimeraX: Structure visualization for researchers, educators, and developers. Protein Science *30*, 70–82. https://doi.org/10.1002/pro.3943.
74. Croll, T.I. (2018). ISOLDE: a physically realistic environment for model building into low-resolution electron-density maps. Acta Crystallogr D Struct Biol *74*, 519–530. https://doi.org/10.1107/S2059798318002425.
75. Jo, S., Kim, T., Iyer, V.G., and Im, W. (2008). CHARMM-GUI: A web-based graphical user interface for CHARMM. Journal of Computational Chemistry *29*, 1859–1865. https://doi.org/10.1002/jcc.20945.
76. Lee, J., Cheng, X., Swails, J.M., Yeom, M.S., Eastman, P.K., Lemkul, J.A., Wei, S., Buckner, J., Jeong, J.C., Qi, Y., et al. (2016). CHARMM-GUI Input Generator for NAMD, GROMACS, AMBER, OpenMM, and CHARMM/OpenMM Simulations Using the CHARMM36 Additive Force Field. J Chem Theory Comput *12*, 405–413. https://doi.org/10.1021/acs.jctc.5b00935.
77. Qi, Y., Ingólfsson, H.I., Cheng, X., Lee, J., Marrink, S.J., and Im, W. (2015). CHARMM-GUI Martini Maker for Coarse-Grained Simulations with the Martini Force Field. J Chem Theory Comput *11*, 4486–4494. https://doi.org/10.1021/acs.jctc.5b00513.
78. Lomize, A.L., Todd, S.C., and Pogozheva, I.D. (2022). Spatial arrangement of proteins in planar and curved membranes by PPM 3.0. Protein Sci *31*, 209–220. https://doi.org/10.1002/pro.4219.
79. Abraham, M.J., Murtola, T., Schulz, R., Páll, S., Smith, J.C., Hess, B., and Lindahl, E. (2015). GROMACS: High performance molecular simulations through multi-level parallelism from laptops to supercomputers. SoftwareX *1–2*, 19–25. https://doi.org/10.1016/j.softx.2015.06.001.
80. Michaud-Agrawal, N., Denning, E.J., Woolf, T.B., and Beckstein, O. (2011). MDAnalysis: A toolkit for the analysis of molecular dynamics simulations. Journal of Computational Chemistry *32*, 2319–2327. https://doi.org/10.1002/jcc.21787.
81. Gowers, R.J., Linke, M., Barnoud, J., Reddy, T.J.E., Melo, M.N., Seyler, S.L., Domański, J., Dotson, D.L., Buchoux, S., Kenney, I.M., et al. (2016). MDAnalysis: A Python Package for the Rapid Analysis of Molecular Dynamics Simulations. Proceedings of the 15th Python in Science Conference, 98–105.

https://doi.org/10.25080/Majora-629e541a-00e.

82. Madeira, F., Pearce, M., Tivey, A.R.N., Basutkar, P., Lee, J., Edbali, O., Madhusoodanan, N., Kolesnikov, A., and Lopez, R. (2022). Search and sequence analysis tools services from EMBL-EBI in 2022. Nucleic Acids Res *50*, W276–W279. https://doi.org/10.1093/nar/gkac240.
83. Letunic, I., and Bork, P. (2024). Interactive Tree of Life (iTOL) v6: recent updates to the phylogenetic tree display and annotation tool. Nucleic Acids Research, gkae268. https://doi.org/10.1093/nar/gkae268.
84. Robert, X., and Gouet, P. (2014). Deciphering key features in protein structures with the new ENDscript server. Nucleic Acids Research *42*, W320–W324. https://doi.org/10.1093/nar/gku316.
85. Tamura, K., Stecher, G., and Kumar, S. (2021). MEGA11: Molecular Evolutionary Genetics Analysis Version 11. Molecular Biology and Evolution *38*, 3022–3027. https://doi.org/10.1093/molbev/msab120.
86. Nye, J., Buster, D.W., and Rogers, G.C. (2014). The use of cultured Drosophila cells for studying the microtubule cytoskeleton. Methods Mol Biol *1136*, 81–101. https://doi.org/10.1007/978-1-4939-0329-0_6.
87. Nishida, K.M., Iwasaki, Y.W., Murota, Y., Nagao, A., Mannen, T., Kato, Y., Siomi, H., and Siomi, M.C. (2015). Respective functions of two distinct Siwi complexes assembled during PIWI-interacting RNA biogenesis in Bombyx germ cells. Cell Rep *10*, 193–203. https://doi.org/10.1016/j.celrep.2014.12.013.
88. Miyoshi, K., Tsukumo, H., Nagami, T., Siomi, H., and Siomi, M.C. (2005). Slicer function of Drosophila Argonautes and its involvement in RISC formation. Genes Dev *19*, 2837–2848. https://doi.org/10.1101/gad.1370605.
89. Saito, K., Ishizuka, A., Siomi, H., and Siomi, M.C. (2005). Processing of pre-microRNAs by the Dicer-1-Loquacious complex in Drosophila cells. PLoS Biol *3*, e235. https://doi.org/10.1371/journal.pbio.0030235.
90. Mirdita, M., Schütze, K., Moriwaki, Y., Heo, L., Ovchinnikov, S., and Steinegger, M. (2022). ColabFold: making protein folding accessible to all. Nat Methods *19*, 679–682. https://doi.org/10.1038/s41592-022-01488-1.
91. Souza, P.C.T., Alessandri, R., Barnoud, J., Thallmair, S., Faustino, I., Grünewald, F., Patmanidis, I., Abdizadeh, H., Bruininks, B.M.H., Wassenaar, T.A., et al. (2021). Martini 3: a general purpose force field for coarse-grained molecular dynamics. Nat Methods *18*, 382–388. https://doi.org/10.1038/s41592-021-01098-3.
92. Lambkin, C.L., Sinclair, B.J., Pape, T., Courtney, G.W., Skevington, J.H., Meier, R., Yeates, D.K., Blagoderov, V., and Wiegmann, B.M. (2013). The phylogenetic

relationships among infraorders and superfamilies of Diptera based on morphological evidence. Systematic Entomology *38*, 164–179. https://doi.org/10.1111/j.1365-3113.2012.00652.x.

93. Misof, B., Liu, S., Meusemann, K., Peters, R.S., Donath, A., Mayer, C., Frandsen, P.B., Ware, J., Flouri, T., Beutel, R.G., et al. (2014). Phylogenomics resolves the timing and pattern of insect evolution. Science *346*, 763–767. https://doi.org/10.1126/science.1257570.
94. Saitou, N., and Nei, M. (1987). The neighbor-joining method: a new method for reconstructing phylogenetic trees. Mol Biol Evol *4*, 406–425. https://doi.org/10.1093/oxfordjournals.molbev.a040454.

Figure 1

Koga et al.

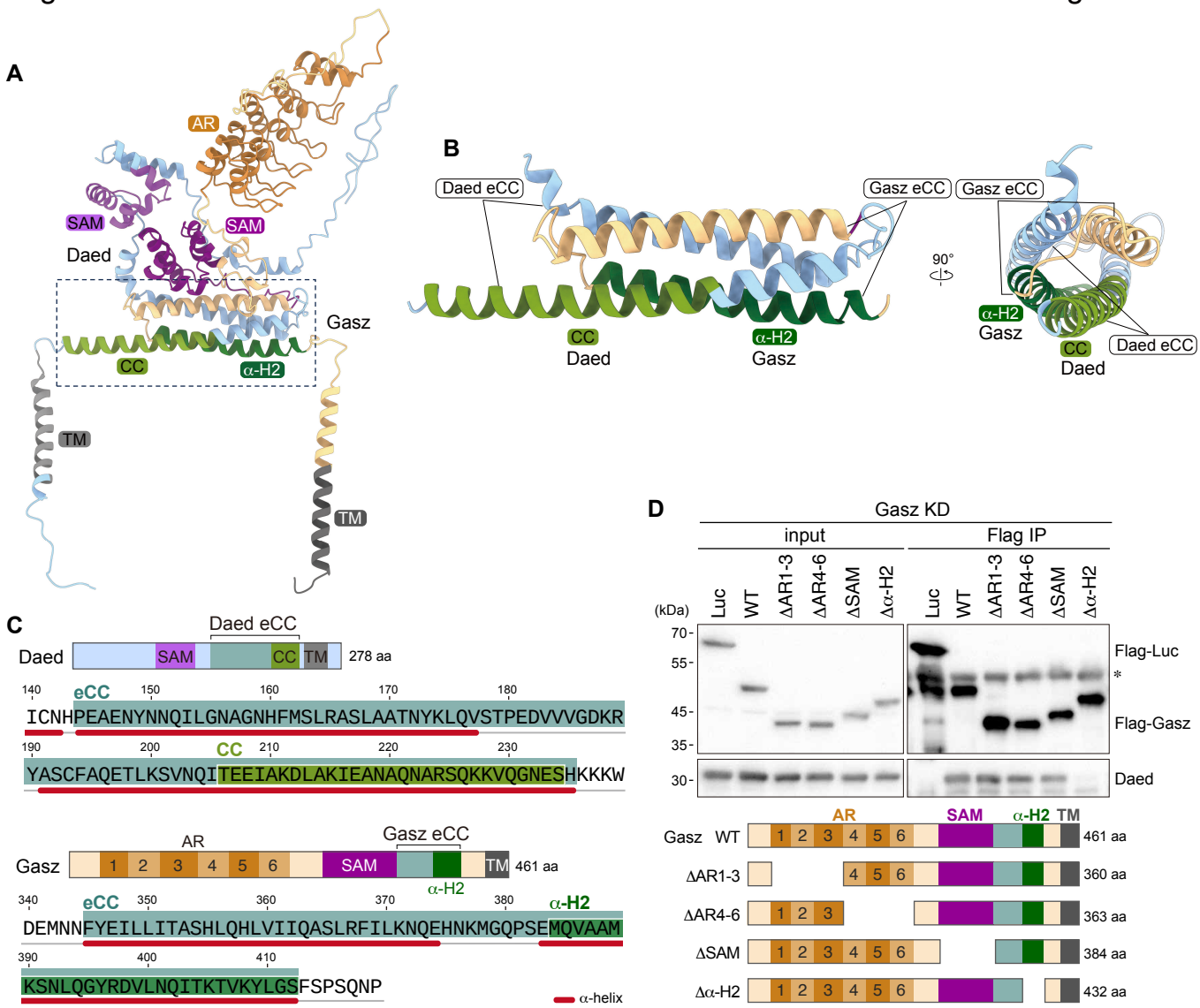

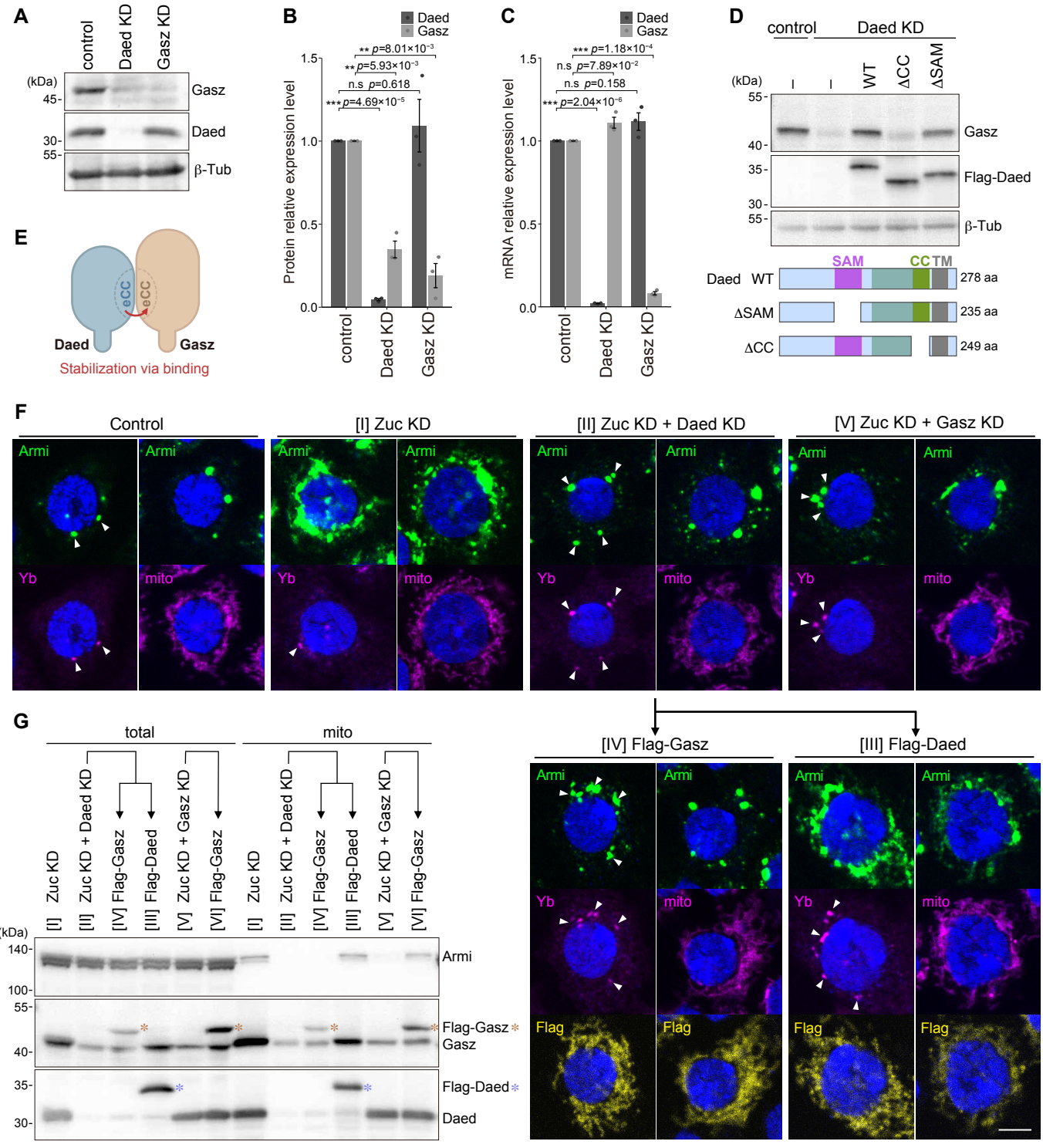
A
control
Daed KD
Gasz KD
(kDa)
45-
30-
55-
Gasz
Daed
β-Tub
B
Daed
Gasz
Protein relative expression level
** p=8.01×10⁻³
** p=5.93×10⁻³
n.s p=0.618
*** p=4.69×10⁻⁵
control
Daed KD
Gasz KD
C
mRNA relative expression level
*** p=1.18×10⁻⁴
n.s p=7.89×10⁻²
n.s p=0.158
*** p=2.04×10⁻⁶
D
control
Daed KD
WT
ΔCC
ΔSAM
55-
40-
35-
30-
Flag-Daed
E
eCC
Daed
Gasz
Stabilization via binding
SAM
CC
TM
Daed WT
278 aa
ΔSAM
235 aa
ΔCC
249 aa
F
Control
[I] Zuc KD
[II] Zuc KD + Daed KD
[V] Zuc KD + Gasz KD
Armi
Yb
mito
G
total
mito
[I] Zuc KD
[II] Zuc KD + Daed KD
[IV] Flag-Gasz
[III] Flag-Daed
[V] Zuc KD + Gasz KD
[VI] Flag-Gasz
140-
100-
Armi
Flag-Gasz
Gasz
Flag-Daed
Daed
[IV] Flag-Gasz
[III] Flag-Daed
Flag

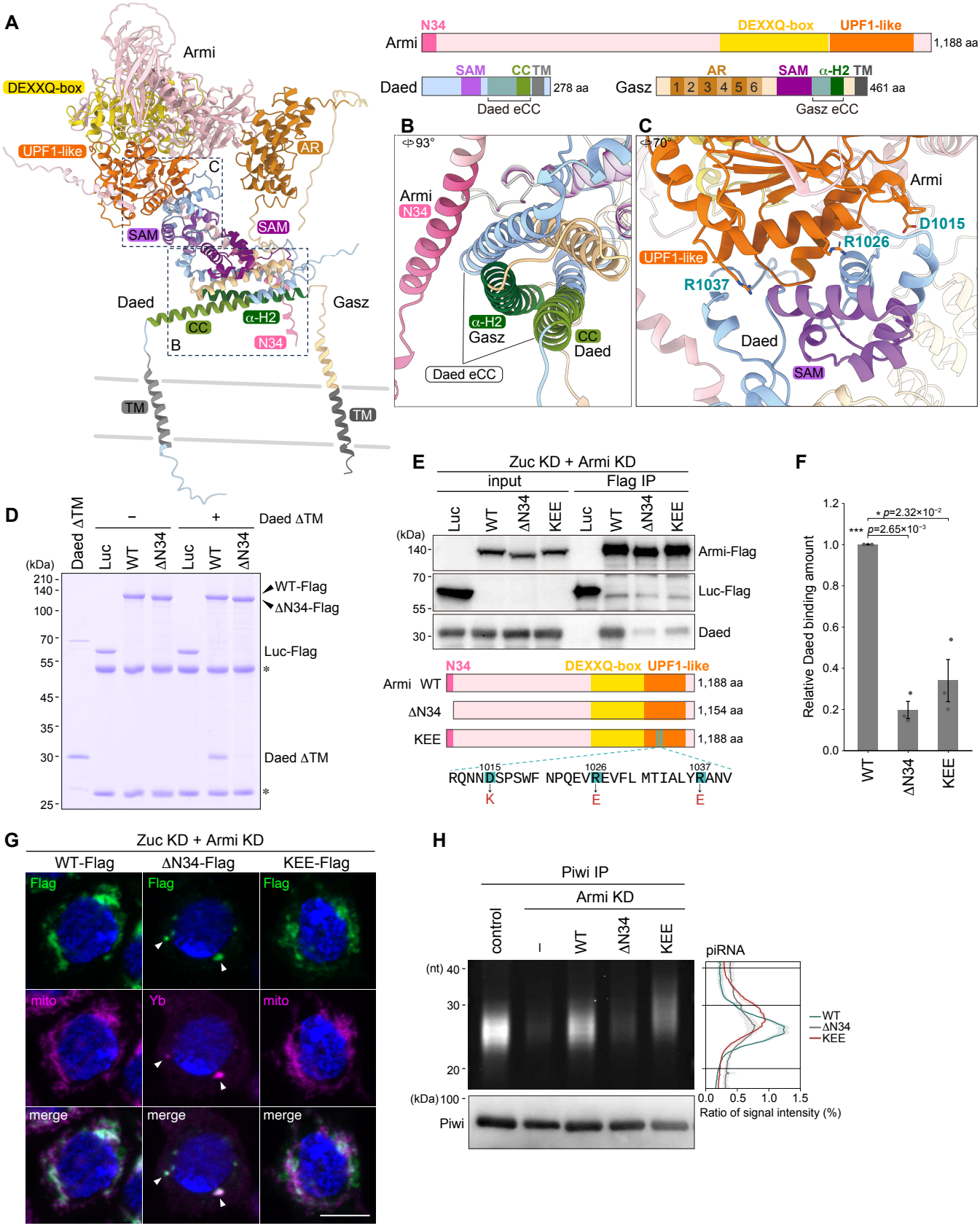
A
Armi
DEXXQ-box
UPF1-like
AR
C
SAM
SAM
Daed
Gasz
α-H2
CC
N34
B
TM
TM
N34
DEXXQ-box
UPF1-like
Armi
1,188 aa
SAM
CC TM
Daed
278 aa
Daed eCC
AR
SAM
α-H2 TM
Gasz
1 2 3 4 5 6
461 aa
Gasz eCC
B
93°
Armi
N34
α-H2
Gasz
CC
Daed
Daed eCC
C
70°
Armi
D1015
R1026
UPF1-like
R1037
Daed
SAM
D
Daed ΔTM
−
+
Daed ΔTM
Luc
WT
ΔN34
Luc
WT
ΔN34
(kDa)
210
140
100
70
55
45
35
30
25
WT-Flag
ΔN34-Flag
Luc-Flag
*
Daed ΔTM
*
E
Zuc KD + Armi KD
input
Flag IP
Luc
WT
ΔN34
KEE
Luc
WT
ΔN34
KEE
(kDa)
140
70
55
30
Armi-Flag
Luc-Flag
Daed
N34
DEXXQ-box
UPF1-like
Armi WT
1,188 aa
ΔN34
1,154 aa
KEE
1,188 aa
1015
1026
1037
RQNNDSPSWF NPQEVREVFL MTIALYRANV
K
E
E
F
Relative Daed binding amount
1.2
1.0
0.8
0.6
0.4
0.2
0.0
* p=2.32×10⁻²
*** p=2.65×10⁻³
WT
ΔN34
KEE
G
Zuc KD + Armi KD
WT-Flag
ΔN34-Flag
KEE-Flag
Flag
Flag
Flag
mito
Yb
mito
merge
merge
merge
H
Piwi IP
Armi KD
control
−
WT
ΔN34
KEE
(nt) 40
30
20
(kDa) 100
Piwi
piRNA
WT
ΔN34
KEE
0.0
0.5
1.0
1.5
Ratio of signal intensity (%)

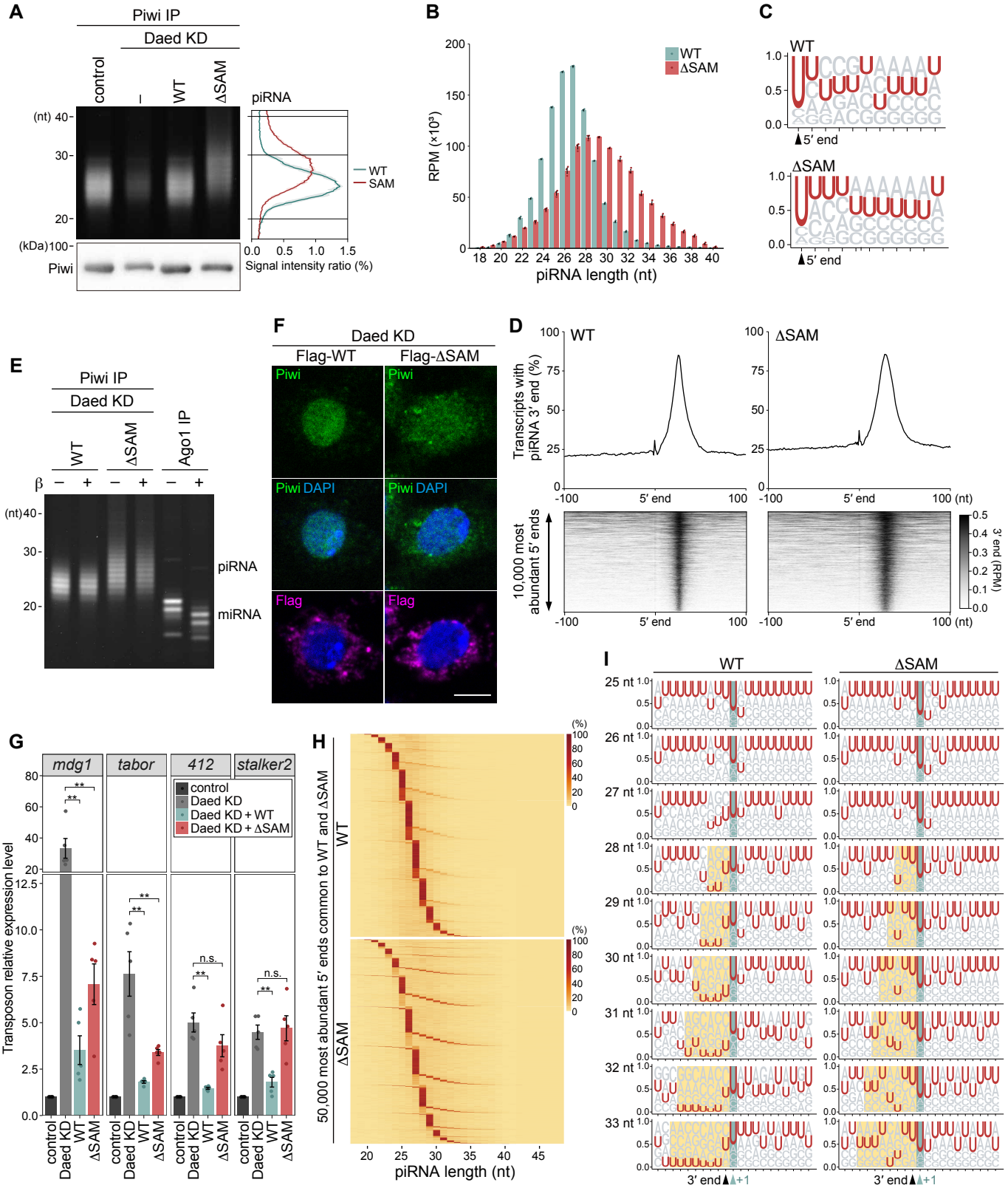
A
Piwi IP
Daed KD
control
I
WT
ΔSAM
(nt) 40
30
20
(kDa) 100
Piwi
piRNA
WT
SAM
0.0 0.5 1.0 1.5
Signal intensity ratio (%)
B
WT
ΔSAM
RPM (×10³)
piRNA length (nt)
C
WT
ΔSAM
5′ end
D
WT
ΔSAM
Transcripts with piRNA 3′ end (%)
5′ end
10,000 most abundant 5′ ends
3′ end (RPM)
E
Piwi IP
Daed KD
WT
ΔSAM
Ago1 IP
β
(nt) 40
30
20
piRNA
miRNA
F
Daed KD
Flag-WT
Flag-ΔSAM
Piwi
Piwi DAPI
Flag
G
mdg1
tabor
412
stalker2
control
Daed KD
Daed KD + WT
Daed KD + ΔSAM
Transposon relative expression level
n.s.
H
50,000 most abundant 5′ ends common to WT and ΔSAM
WT
ΔSAM
(%)
piRNA length (nt)
I
WT
ΔSAM
25 nt
26 nt
27 nt
28 nt
29 nt
30 nt
31 nt
32 nt
33 nt
3′ end
+1

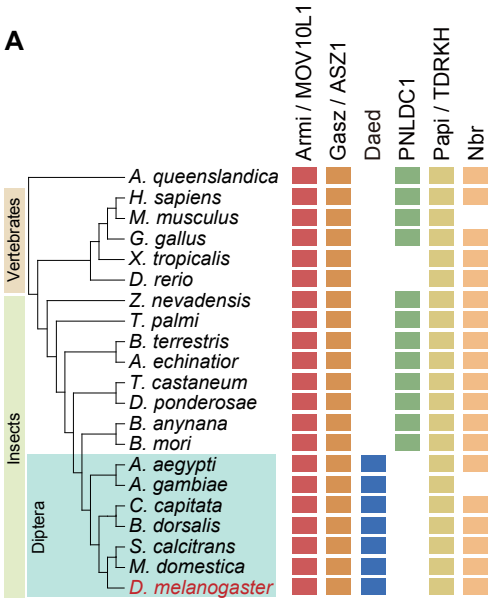
A
Armi / MOV10L1
Gasz / ASZ1
Daed
PNLDC1
Papi / TDRKH
Nbr
Vertebrates
Insects
Diptera
A. queenslandica
H. sapiens
M. musculus
G. gallus
X. tropicalis
D. rerio
Z. nevadensis
T. palmi
B. terrestris
A. echinatior
T. castaneum
D. ponderosae
B. anynana
B. mori
A. aegypti
A. gambiae
C. capitata
B. dorsalis
S. calcitrans
M. domestica
D. melanogaster

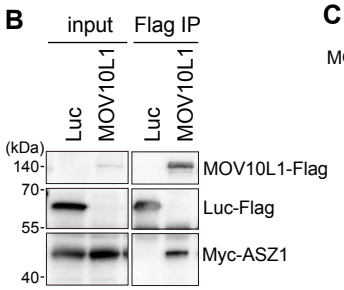
B
input
Flag IP
Luc
MOV10L1
Luc
MOV10L1
(kDa)
140
70
55
40
MOV10L1-Flag
Luc-Flag
Myc-ASZ1

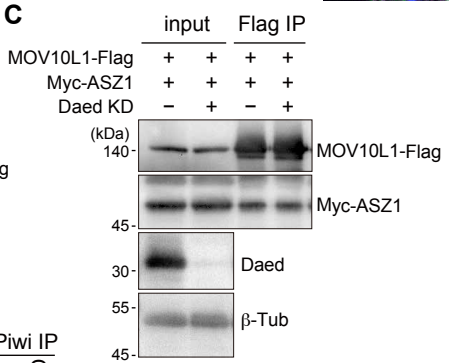
C
input
Flag IP
MOV10L1-Flag + + + +
Myc-ASZ1 + + + +
Daed KD − + − +
(kDa)
140
45
30
55
45
MOV10L1-Flag
Myc-ASZ1
Daed
β-Tub

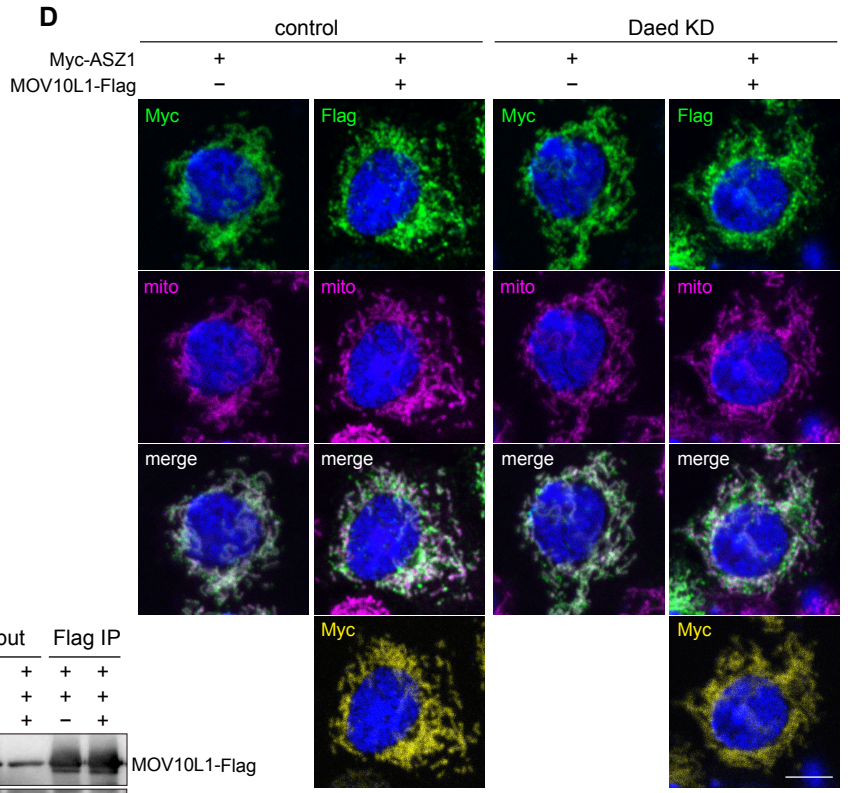
D
control
Daed KD
Myc-ASZ1 + + + +
MOV10L1-Flag − + − +
Myc
Flag
Myc
Flag
mito
mito
mito
mito
merge
merge
merge
merge
Myc
Myc

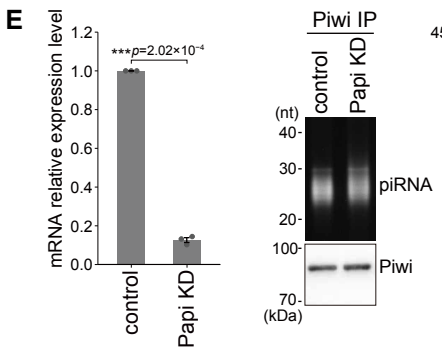
E
mRNA relative expression level
***p=2.02×10⁻⁴
1.2
1.0
0.8
0.6
0.4
0.2
0.0
control
Papi KD
Piwi IP
control
Papi KD
(nt)
40
30
20
100
70
(kDa)
piRNA
Piwi

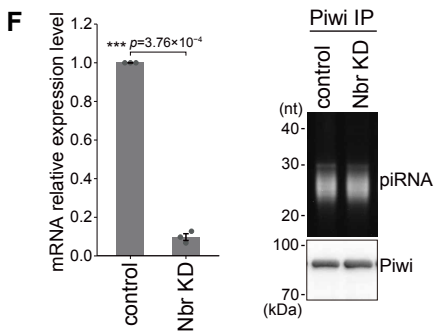
F
mRNA relative expression level
*** p=3.76×10⁻⁴
1.2
1.0
0.8
0.6
0.4
0.2
0.0
control
Nbr KD
Piwi IP
control
Nbr KD
(nt)
40
30
20
100
70
(kDa)
piRNA
Piwi

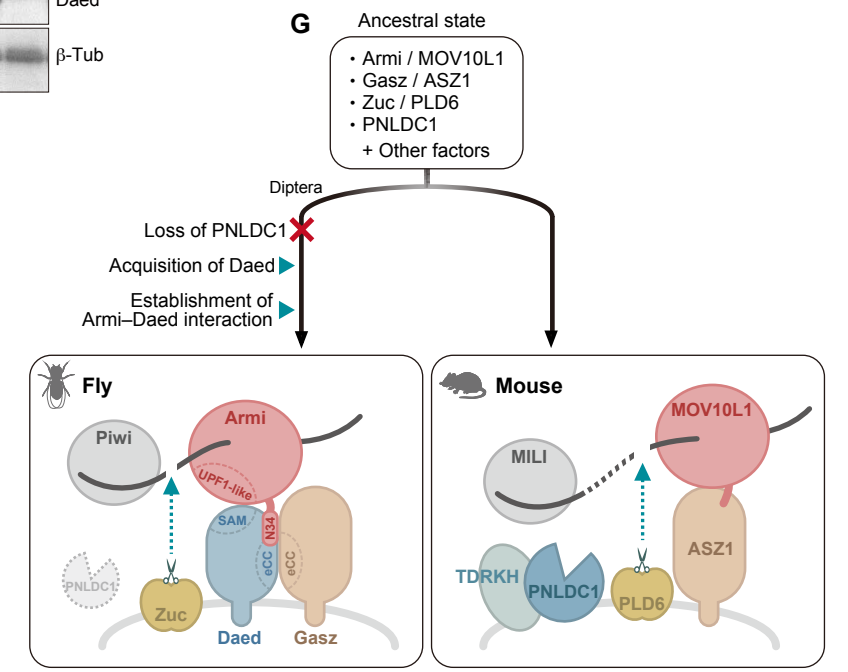
G
Ancestral state
• Armi / MOV10L1
• Gasz / ASZ1
• Zuc / PLD6
• PNLDC1
+ Other factors
Diptera
Loss of PNLDC1
Acquisition of Daed
Establishment of
Armi–Daed interaction
Fly
Piwi
Armi
UPF1-like
SAM
N34
eCC
eCC
PNLDC1
Zuc
Daed
Gasz
Mouse
MOV10L1
MILI
ASZ1
TDRKH
PNLDC1
PLD6

Supplemental information

Diptera-specific Daedalus controls Zucchini endonucleolysis in piRNA biogenesis independent of exonucleases

Yuica Koga, Shigeki Hirakata, Mayu Negishi, Hiroya Yamazaki, and Mikiko C. Siomi*

Department of Biological Sciences, Graduate School of Science, The University of Tokyo, Tokyo 113-0032, Japan

*Correspondence: siomim@bs.s.u-tokyo.ac.jp

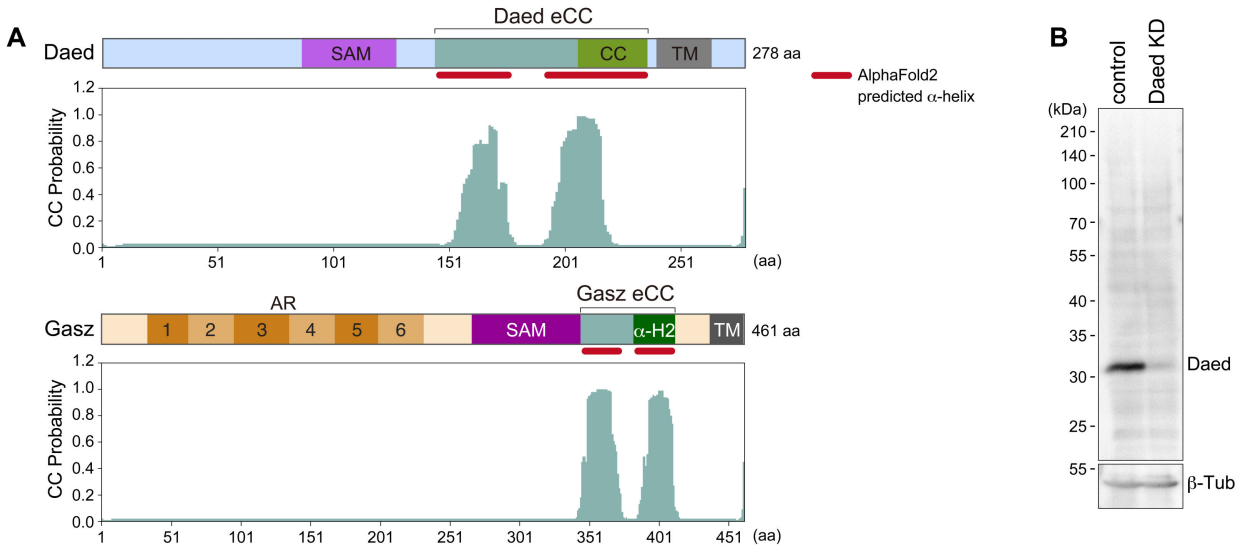

Figure S1. Related to Figure 1; Coiled-coil prediction and specificity of anti-Daed antibodies

(**A**) Sequence-based CC prediction of Daed (upper) and Gasz (lower) by CoCoNat. Red line indicates the CC region predicted by AlphaFold2. (**B**) Western blotting shows that anti-Daed monoclonal antibodies produced in this study are specific to Daed. Daed KD: Daed knockdown by RNAi. control: EGFP KD. β-Tub: loading control.

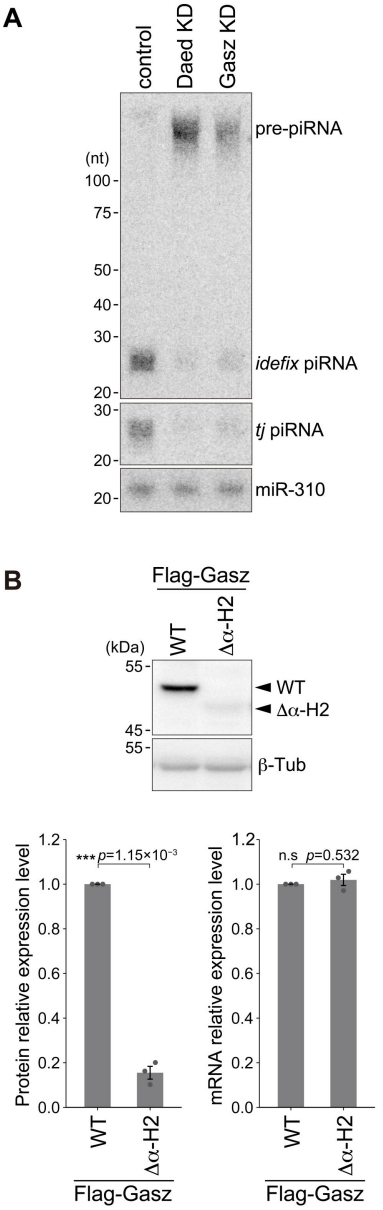

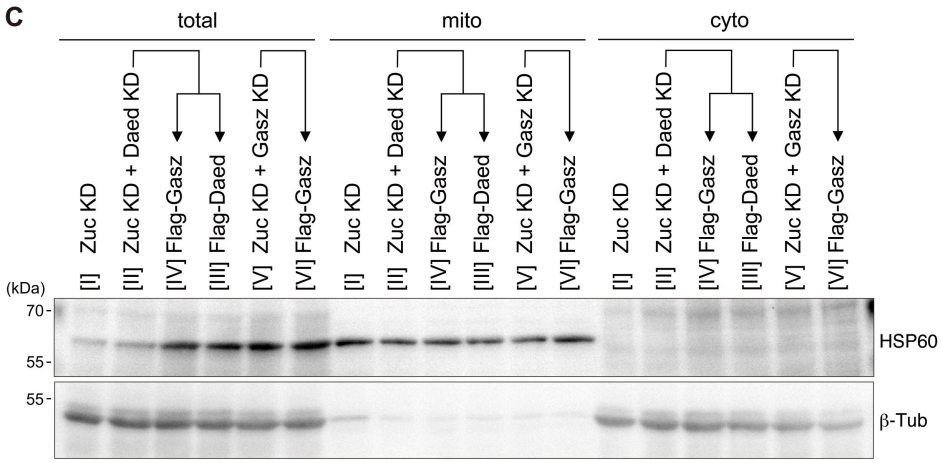

D

	Armi	Daed	Gasz
Control	Yb body	+	+
[I] Zuc KD	mitochondria	+	+
[II] ZucKD + Daed KD	Yb body	–	–
[III] ZucKD + Daed KD, Flag-Daed	mitochondria	+	+
[IV] ZucKD + Daed KD, Flag-Gasz	Yb body	–	+
[V] ZucKD + Gasz KD	Yb body	+	–
[VI] ZucKD + Gasz KD, Flag-Gasz	mitochondria	+	+

Figure S2. Related to Figure 2; Functions and behaviors of Daed and Gasz in OSCs

(**A**) Northern blotting using probes that detect *idefix* piRNA and *tj* piRNA. miR-310: loading control. KD: knockdown by RNAi. control: EGFP KD. pre-piRNA: piRNA precursors. (**B**) Western blotting shows the levels of Flag-Gasz WT and Flag-Gasz Δα-H2 where the same amounts of plasmids were used for transfection. β-Tub: loading control. The statistics of western blotting signals (n=3; left) and the mRNA expression levels (n=3; right). Signal intensities (left) or values (right) relative to F-Gasz WT were normalized with those of β-Tub or *rp49*, respectively, and presented as mean values±SE. ***: p <0.005;

n.s.: $p > 0.05$ [*t*-test (unpaired, two-sided)]. (**C**) Western blotting shows HSP60 (a mitochondrial fraction marker) and β-Tub (a cytoplasmic fraction marker) in total lysates, and mitochondrial and cytoplasmic fractions in Figure 2G. (**D**) Summary of Armi subcellular localization in OSCs under each condition.

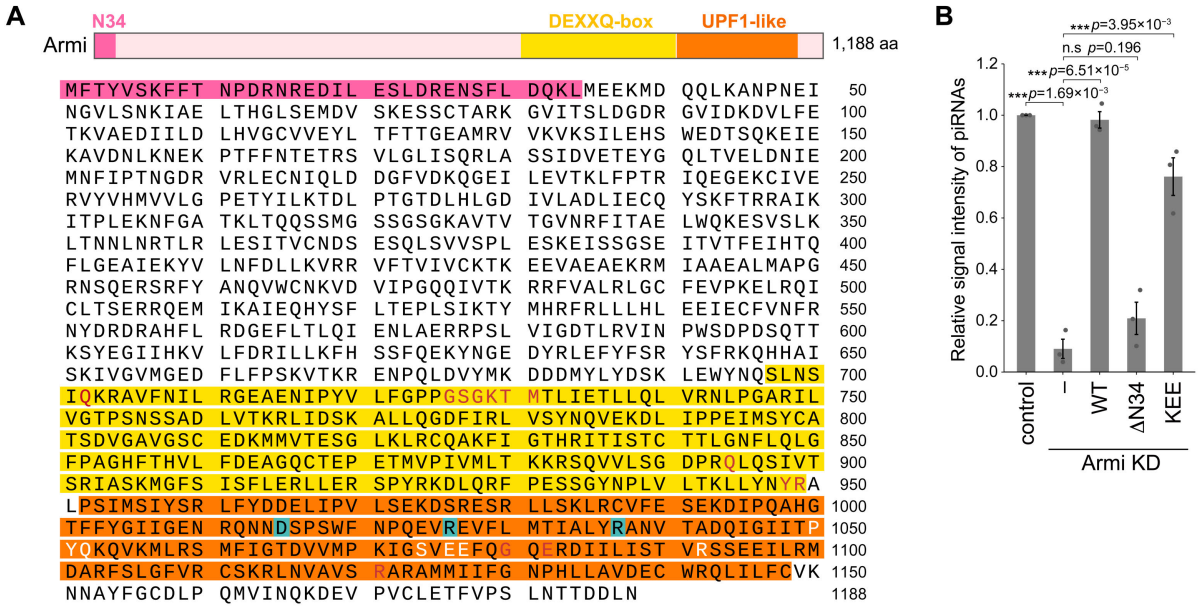

Figure S3. Related to Figure 3; Effects of Armi mutants on piRNA biogenesis

(**A**) Peptide sequence and domain structure of Armi. The ATP binding residues and nucleotide binding residues are indicated in red and white, respectively. Asp1015, Arg1026, and Arg1037 are highlighted in blue. (**B**) Quantification of piRNA levels (n=3) (Figure 3H). Values relative to the control (EGFP KD) were normalized to Piwi level and presented as mean values ± SE. ***: $p < 0.005$; n.s.: $p > 0.05$ [*t*-test (unpaired, two-sided)].

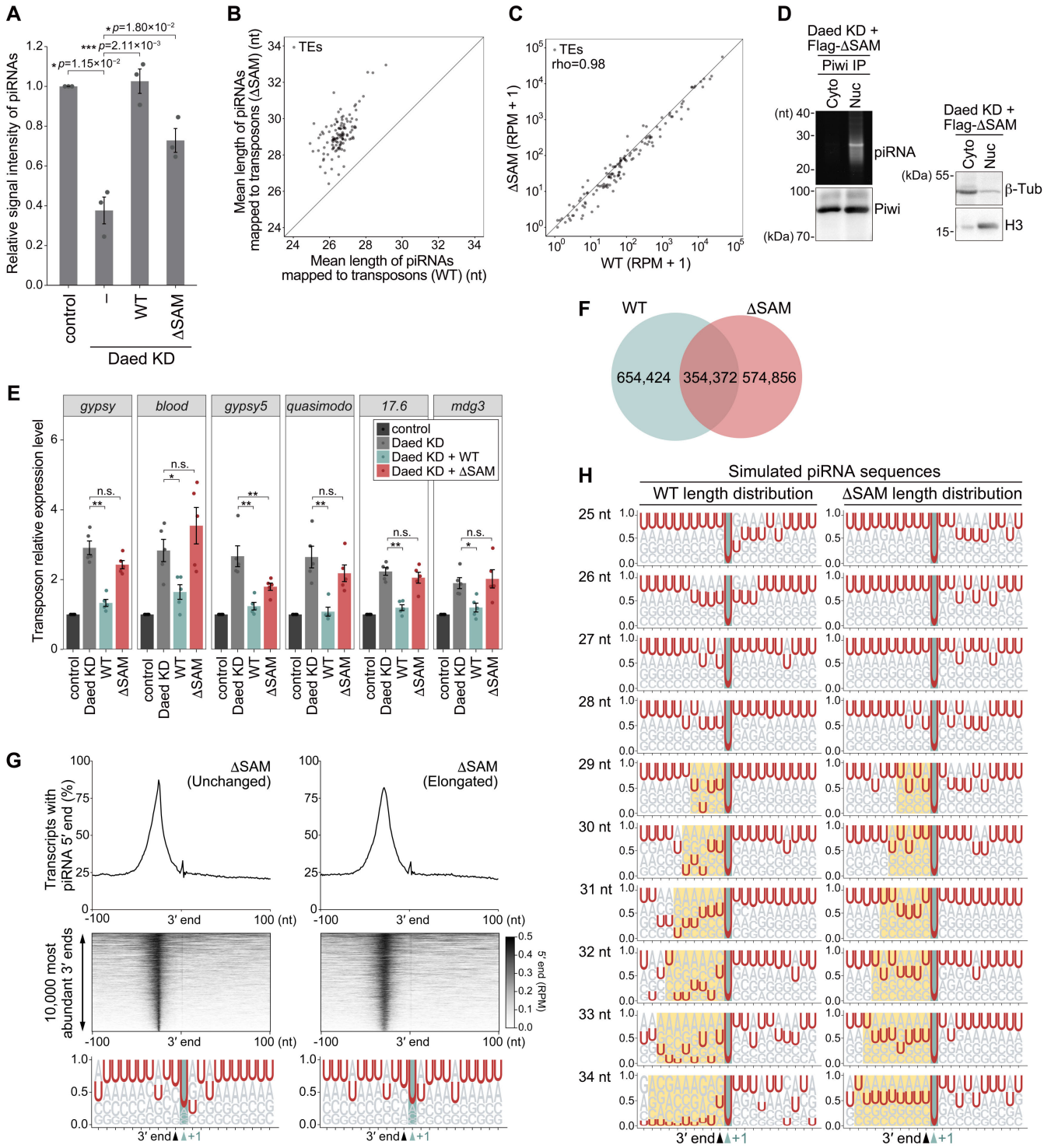

Figure S4. Related to Figure 4; Effects of Daed ΔSAM on piRNA biogenesis and Piwi-piRISC

function

(**A**) Quantification of piRNA levels (n=3) (Figure 4A). Values relative to the control (EGFP KD) were normalized to Piwi level and presented as mean values ± SE. ***: $p < 0.005$; *: $p < 0.05$; [*t*-test (unpaired, two-sided)]. (**B**, **C**) Scatter plots showing the length distribution of piRNAs upon subdivision by target transposons (**B**) and the abundance of reads mapped antisense to transposons (**C**; Spearman's rho=0.98) in Daed WT and ΔSAM libraries. (**D**) Left: Piwi-bound piRNAs obtained from cytoplasmic fraction (Cyto) and nuclear extract fraction (Nuc). Immunoprecipitated Piwi was detected by western blotting. Right: Western blotting showing β-Tub (a cytoplasmic marker) and Histon H3 (a nucleus marker) in each fraction. (**E**) The expression levels of transposons (*gypsy*, *blood*, *gypsy5*, *quasimodo*, *17.6*, and *mdg3*) in control OSCs (dark gray), Daed-lacking OSCs (Daed KD; light gray), Flag-Daed WT rescued (WT; green) or Flag-Daed ΔSAM rescued cells (ΔSAM; red) (n=5). Values relative to the control (EGFP KD) were normalized to *rp49* and presented as mean values ± SE **: $p < 0.01$; *: $p < 0.05$; n.s.: $p > 0.05$ [Wilcoxon rank sum exact test (two-sided)]. (**F**) Venn diagram showing the variety of positions of piRNA 5′ ends in the WT and ΔSAM libraries. (**G**) Heatmaps showing 5′ end counts of piRNAs mapped around the 10,000 most abundant piRNA 3′ ends (middle) and its binary histogram (top). In sequence logos (bottom), piRNAs were aligned according to the 3′ end of the piRNAs (black arrowhead) and its immediately downstream nucleotide is highlighted in green. Left: Daed ΔSAM piRNAs in "Unchanged" group. Right: Daed ΔSAM piRNAs in "Elongated" group. (**H**) piRNA production simulation. The U depletion in 29–34-nt piRNAs in WT and equivalent regions in ΔSAM are highlighted in yellow.

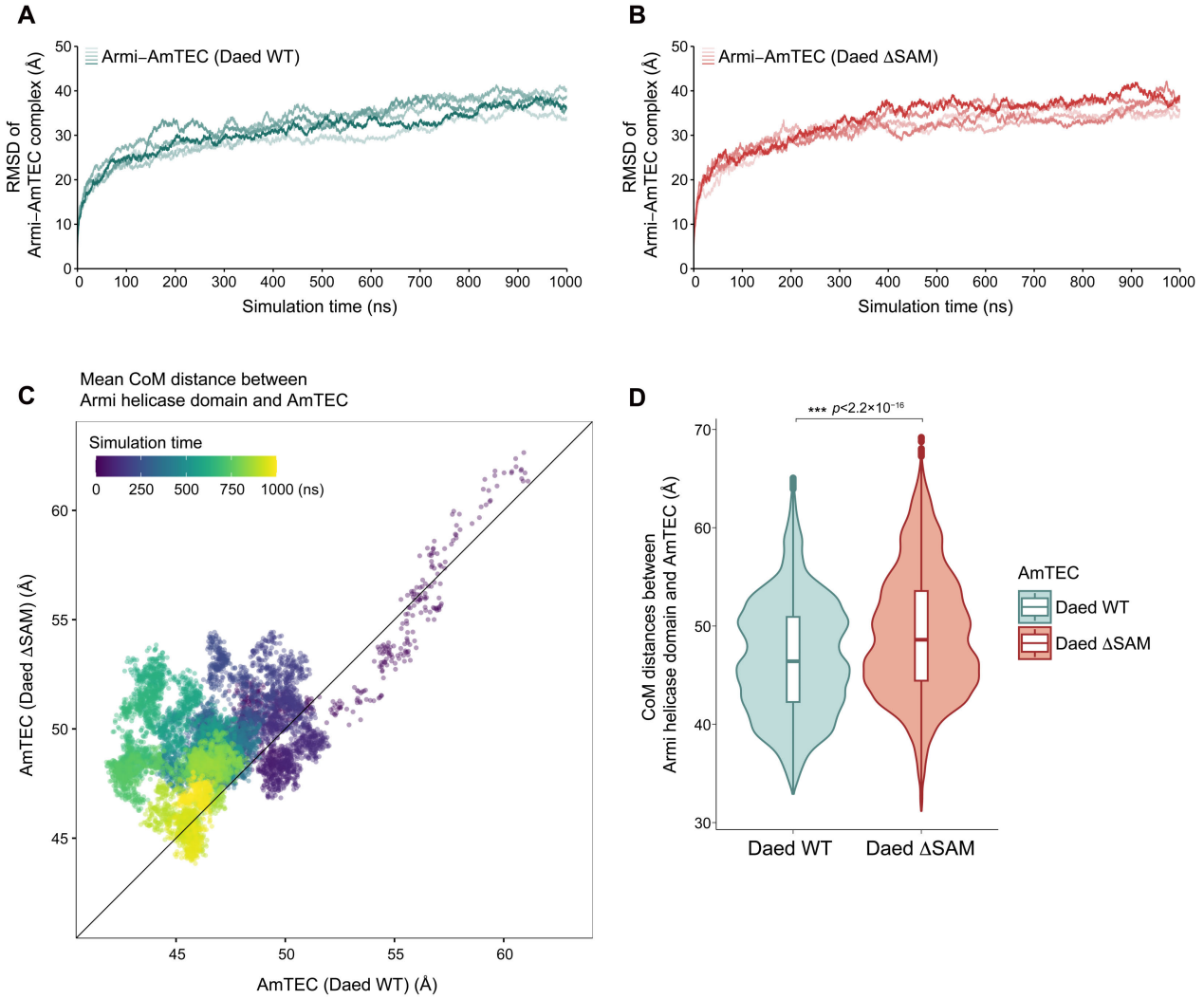

Figure S5. Related to Figure 4; MD simulation of Armi–AmTEC complex

(**A**, **B**) Root mean square deviation (RMSD) of the Armi–AmTEC complex (**A**) and its Daed ΔSAM version (**B**) in molecular dynamics simulations (n=5) indicates that the simulation reaches equilibrium state over the simulation time. (**C**) The average distance between the center of mass (CoM) of Armi helicase domain and that of AmTEC (n=5) for each time point of the trajectory is shown. (**D**) Violin plot of CoM distances between Armi helicase domain and AmTEC (blue) and its Daed ΔSAM version (red) for all time points in all trajectories. ***: $p < 0.005$ [Welch's *t*-test (two-sided)].

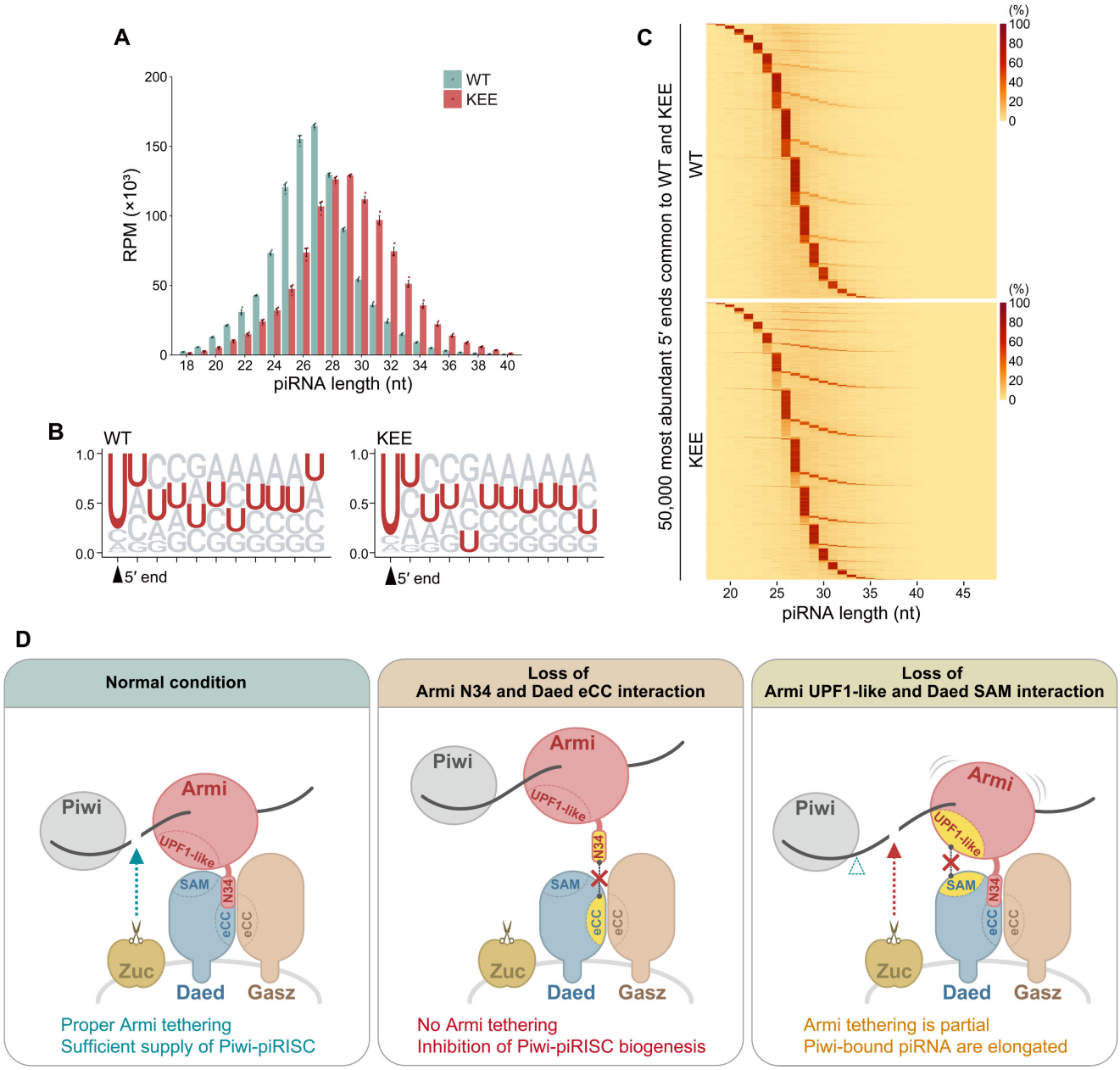

Figure S6. Related to Figure 4; Effects of Armi KEE on piRNA biogenesis

(**A**) Length distribution of piRNAs (18–40 nt) in Armi WT (green) and KEE (red) libraries (n=3), presented as mean values±SE. (**B**) Sequence logos representing 11 nt from the 5′ end of piRNAs in the Armi WT and KEE libraries. (**C**) Heatmaps showing the frequency of the 3′ end positions (red) corresponding to each 5′ end of piRNAs in Armi WT (upper) and KEE (lower) libraries. The 50,000 piRNA 5′ end positions common to both libraries and most abundant in the WT library were used for analysis. (**D**) The model

summarizing the effects of the perturbation of two Armi–AmTEC interactions (Armi N34–Daed eCC and Armi UPF1-like–Daed SAM). Blue arrowhead (left panel): Zuc cleavage. Red arrowhead (right panel): obscured Zuc cleavage. White arrowhead (right panel): Zuc cleavage corresponding to WT. Black dashed line with a red cross (middle and right panel): perturbated interaction.

Figure S7

Koga et al.

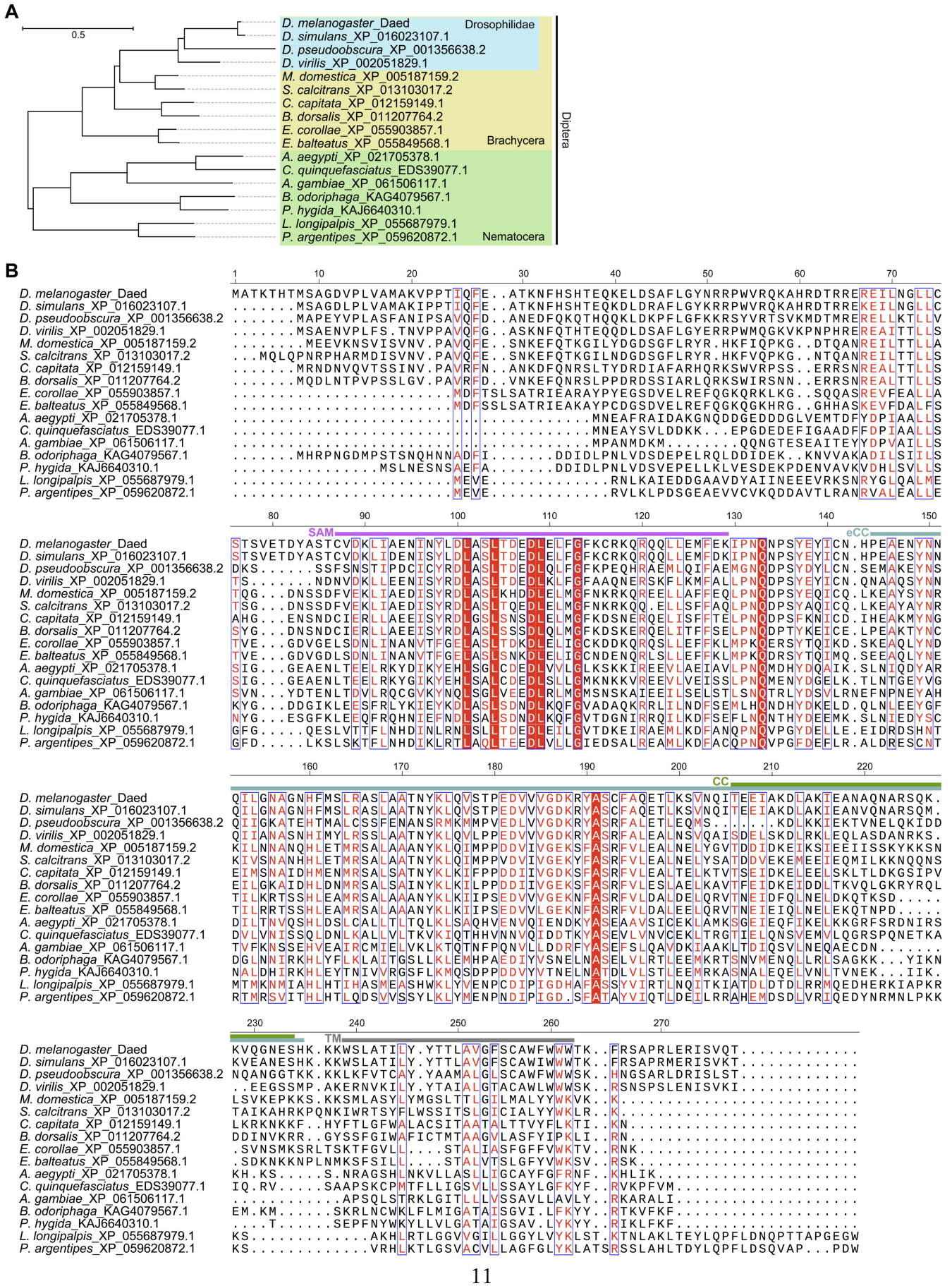

Figure S7. Related to Figure 5; Sequence alignment of Daed in species

(**A**, **B**) Phylogenetic tree (**A**) and multiple sequence alignment (**B**) of Daed orthologs constructed and visualized using Clustal Omega, MEGA 11 and ESPript.

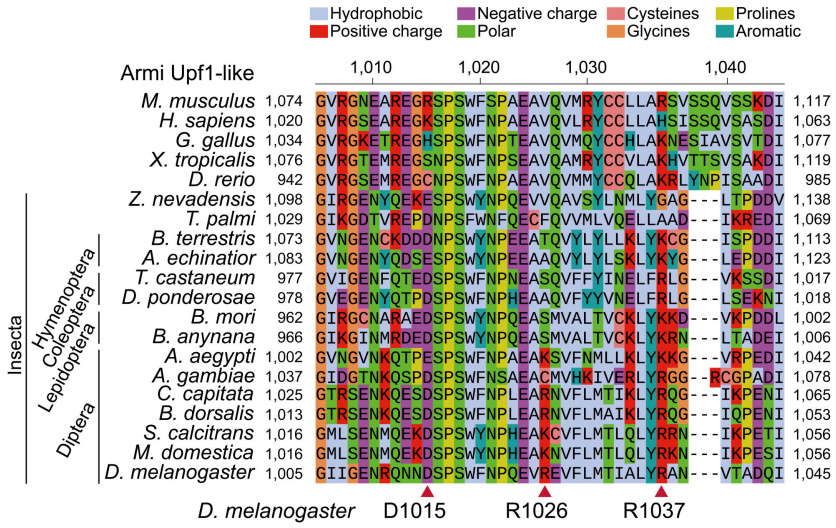

Figure S8. Related to Figure 5; Sequence alignment of Armi UPF1-like helicase domain in species

Multiple sequence alignment of *D. melanogaster* Armi and its orthologs. Red arrowheads: Asp1015, Arg1026, and Arg1037 (D-R-R) of *D. melanogaster* Armi.

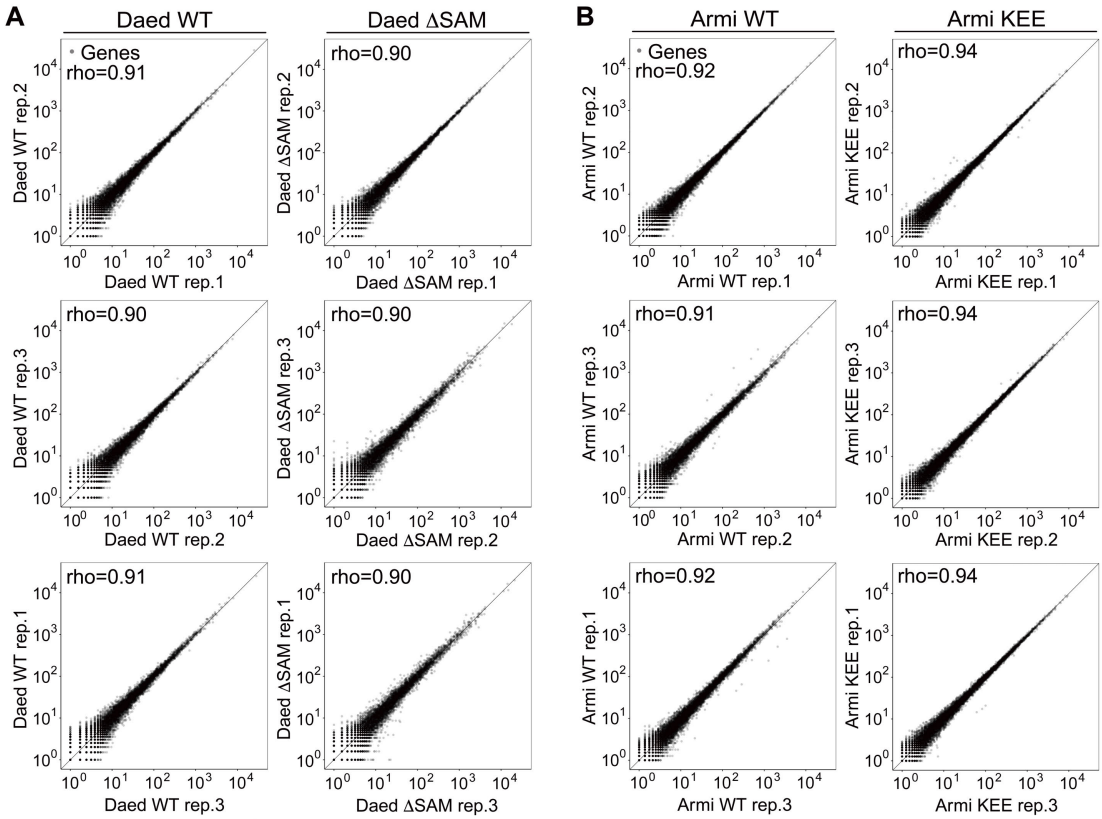

Figure S9. Related to STAR Method "piRNA sequencing and bioinformatic analysis"; Reproducibility of piRNA-seq

(**A,B**) Scatter plots showing reproducibility of piRNA-seq of Daed WT, ΔSAM mutant (**A**), Armi WT and KEE mutant libraries (**B**). Gray dots indicate the number of normalized piRNA reads mapped to coding genes.

Table S1. Related to STAR Method "Plasmid construction"; Sequences of primers used for plasmid construction

name	primer sequence	plasmid
Daed-clonig-insert_F	CTTGGTACCGAATTCATGGCAACGAAGACGCACAC	pAc-Flag-Daed
Daed-clonig-insert_R	GACTCGAGCGGCCGCTTAAGTCTGAACGGAGATCC	pAc-Flag-Daed
Daed-clonig-vector_F	TAAGCGGCCGCTCGAGTCTA	pAc-Flag-Daed
Daed-clonig-vector_R	CATGAATTCGGTACCAAGCT	pAc-Flag-Daed
Flag-Luc_insert_F	ATGGACTACAAAGACCATGACG	pAc-Flag-Luc
Flag-Luc_insert_R	CTTGTCATCGTCATCCTTGT	pAc-Flag-Luc
Flag-Luc_vector_F	GTCTTTGTAGTCCATGGTGGCTAGCCCGAT	pAc-Flag-Luc
Flag-Luc_vector_R	GGATGACGATGACAAGATGGAAGACGCCAAAAACATAAAGAAAG	pAc-Flag-Luc
Flag-Daed (RNAi resistant)_F	GATAAGCTCATTGCCGAGAACATT	pAc-Flag-Daed (RNAi resistant)
Flag-Daed (RNAi resistant)_R	AACGCATGTACTGGCGTAGTCC	pAc-Flag-Daed (RNAi resistant)
Flag-Daed ΔSAM_F	ATTCCCAACCAGAATCCCAGTTACG	pAc-Flag-Daed ΔSAM
Flag-Daed ΔSAM_R	TGTACTGGCGTAGTCCGTTTCCACG	pAc-Flag-Daed ΔSAM
Flag-Daed ΔCC_F	CACAAGAAGAAGAAGTGGAGCCTGG	pAc-Flag-Daed ΔCC
Flag-Daed ΔCC_R	GATCTGATTCACGCTTTTTAGAGTT	pAc-Flag-Daed ΔCC
GST-Daed_full_length_insert_F	GGGCCCCTGGGATCCATGGCAACGAAGACGCACAC	pGEX-GST-Daed
GST-Daed_full_length_insert_R	ACCCGGGAATTCCGGTTAAGTCTGAACGGAGATCC	pGEX-GST-Daed
GST-Daed_full_length_vector_F	CCGGAATTCCCGGGTCGACTCGAGC	pGEX-GST-Daed
GST-Daed_full_length_vector_R	GGATCCCAGGGGCCCCTGGAACAGA	pGEX-GST-Daed
GST-Daed ΔTM_F	TGGACCAAGTTCCGCAGCGCTCCCC	pGEX-GST-Daed ΔTM
GST-Daed ΔTM_R	CTTCTTCTTCTTGTGACTCTCGTTG	pGEX-GST-Daed ΔTM
GST-Daed ΔTM-His_F	CATCATCACTAACCGGAATTCCCGG	pGEX-GST-Daed ΔTM-His
GST-Daed ΔTM-His_R	ATGATGATGAGTCTGAACGGAGATC	pGEX-GST-Daed ΔTM-His
GST-Daed (N1-197)_insert_F	GGGCCCCTGGGATCCATGGCAACGAAGACGCA	pGEX-GST-Daed (N1-197)
GST-Daed (N1-197)_insert_R	ACCCGGGAATTCCGGTTATTCCTGGGCAAAGCAG	pGEX-GST-Daed (N1-197)
GST-Daed (N1-197)_vector_F	CCGGAATTCCCGGGT	pGEX-GST-Daed (N1-197)
GST-Daed (N1-197)_vector_R	GGATCCCAGGGGCC	pGEX-GST-Daed (N1-197)
Flag-Gasz ΔAR1-3_F	CACGGAGCCGTGATCAATGTTTCGG	pAc-Flag-Gasz ΔAR1-3
Flag-Gasz ΔAR1-3_R	CTTGGAGCGTTTCACCTCATCCGAG	pAc-Flag-Gasz ΔAR1-3
Flag-Gasz ΔAR4-6_F	CCAGCCTCCACTTACCTAGTGCCGA	pAc-Flag-Gasz ΔAR4-6
Flag-Gasz ΔAR4-6_R	CCGCAAGAGCAGGCCCACAATTCTC	pAc-Flag-Gasz ΔAR4-6
Flag-Gasz ΔSAM_F	TTCTATGAGATCCTACTGATCACCG	pAc-Flag-Gasz ΔSAM
Flag-Gasz ΔSAM_R	TTGAAAATATTCCGGGCAATCGCTC	pAc-Flag-Gasz ΔSAM
Flag-Gasz ΔCC_F	TTTAGCCCCTCTCAGAATCCCTTGT	pAc-Flag-Gasz ΔCC
Flag-Gasz ΔCC_R	CTCCGAAGGTTGCCCCATTTTATTG	pAc-Flag-Gasz ΔCC
Armi D1015K-Flag_F	ATAACAAATCaCCTTCCTGGTTCAA	pAc-Armi KEE-Flag
Armi D1015K-Flag_R	TTTGCCTGTTTTCGCCAATGATTCC	pAc-Armi KEE-Flag
Armi R1026E-Flag_F	AATCCCCAAGAGGTCGAGGAGGTGT	pAc-Armi KEE-Flag
Armi R1026E-Flag_R	GAACCAGGAAGGTGAATCGTTATTT	pAc-Armi KEE-Flag
Armi R1037E-Flag_F	ACGAGGCCAATGTGACTGCCGATCA	pAc-Armi KEE-Flag
Armi R1037E-Flag_R	ACAGGGCGATGGTCATTAGGAACAC	pAc-Armi KEE-Flag
MOV10L1-clonig-insert_F	ATCGGGCTAGCCACCATGCTGCGCCTTGCTGCCAA	pAc-MOV10L1-Flag
MOV10L1-clonig-insert_R	TTTGTAGTCCTCGAGCTTTTGGAGAGCCTGGAGTT	pAc-MOV10L1-Flag
MOV10L1-clonig-vector_F	CTCGAGGACTACAAAGACCATGACG	pAc-MOV10L1-Flag
MOV10L1-clonig-vector_R	CATGGTGGCTAGCCCGATCCGGGGT	pAc-MOV10L1-Flag
ASZ1-clonig-insert_F	GGTACCGAATTCATGGCAGCGGGCACACTGAGGGG	pAc-Myc-ASZ1
ASZ1-clonig-insert_R	TCGAGCGGCCGCTTATTTTCTCTGCAAAGTTAGCT	pAc-Myc-ASZ1
ASZ1-clonig-vector_F	TAAGCGGCCGCTCGAGTCTAGAGGG	pAc-Myc-ASZ1
ASZ1-clonig-vector_R	CATGAATTCGGTACCAAGCTTGTTC	pAc-Myc-ASZ1

Table S2. Related to STAR Method "RNAi and transfection"; Sequences of siRNAs

name	sense	antisense
siEGFP	*GGCAAGCUGACCCUGAAGU*TT	*ACUUCAGGGUCAGCUUGCC*TT
siDaed	*CCUGUGUGGACAAACUUAUUG*	*AUAAGUUUGUCCACACAGGUG*
siGasz	*CGCUCGAAACCAGCUCCUU*TT	*AAGGAGCUGGUUUCGAGCG*TT
siArmi	*CAGCUUAAGGCGAAUCCAA*TT	*UUGGAUUCGCCUUAAGCUG*TT
siZuc	*GCAUUGCCGUCAGCACUGU*TT	*ACAGUGCUGACGGCAAUGC*TT
siPapi	*GAUUACGAGACAAAGACAG*TT	*CUGUCUUUGUCUCGUAAUC*TT
siNbr	*CCUAAUGAGCAACCTGAAG*TT	*CUUCAGGUUGCUCAUUAGG*TT

*: RNA is shown in itallics

Table S3. Related to STAR Method "Northern blotting"; Sequences of oligos used for northern blotting

name	probe sequence
idefix-piRNA	AAACTACTGGCAATCGTTTGGGAA
tj-piRNA	GGTAATGGGAATGCACTTCTCTTGAA
miR-310	AAAGGCCGGGAAGTGTGCAATA

Table S4. Related to STAR Method "RT-qPCR"; Sequences of primers used for RT-qPCR

name	forward primer (5′ > 3′)	reverse primer (5′ > 3′)
rp49	CCGCTTCAAGGGACAGTATCTG	ATCTCGCCGCAGTAAACGC
Daed	GCAACGAAGACGCACACAAT	TCGGTGTGCGAGTGAAAGTT
Gasz	ACTTCCTGGGCTACAACACG	GGCCTCCAGTATGCCGTTAA
Flag-Gasz	ATGGACTACAAAGACCATGACGGTG	GAGCAGGCCCACAATTCTCTCCGCC
Nbr	GCCTTGGCAAGAAACTGAAC	ACCCCGCCTGAGAAAGTTAT
Papi	GACAGAGGTGGCACATTGGA	GTTCAGAGTTGTCGGCTGGA
mdg1	AACAGAAACGCCAGCAACAGC	CGTTCCCATGTCCGTTGTGAT
tabor	ACAACAGAAGCCGCAAACTG	CAGCTATTGTGAGTGGGCGT
412	ATGCCACTGGTCTAAGCACC	ATAGTGGTGCAAGTCCCTGC
stalker2	CACACAGAAGAACAAGCGGC	TTAACCGCAACGCTTCCTCT
gypsy	GAACCGGTGTACTCAAGAGC	CCAGGTCGGGCTGTTATAGG
blood	AAGACTGCCCTCGACCATTG	ATTCGCTGTTGTCATGTGCG
quasimodo	CCCGACAACAGACAAGAGGC	AGCCCAAGTGTTGCACTGTT
gypsy5	GCCCAGAGACAACGACAGAA	CTGTCTTTGCTGTCCCGGAT
17.6	AATTGGCGCAGTCGATGTGA	TGCCCGTTATCGTGGTACTT
mdg3	ATGCCATACGATGCGCAAAC	CGCTCTTCCTTGTGGGACAT